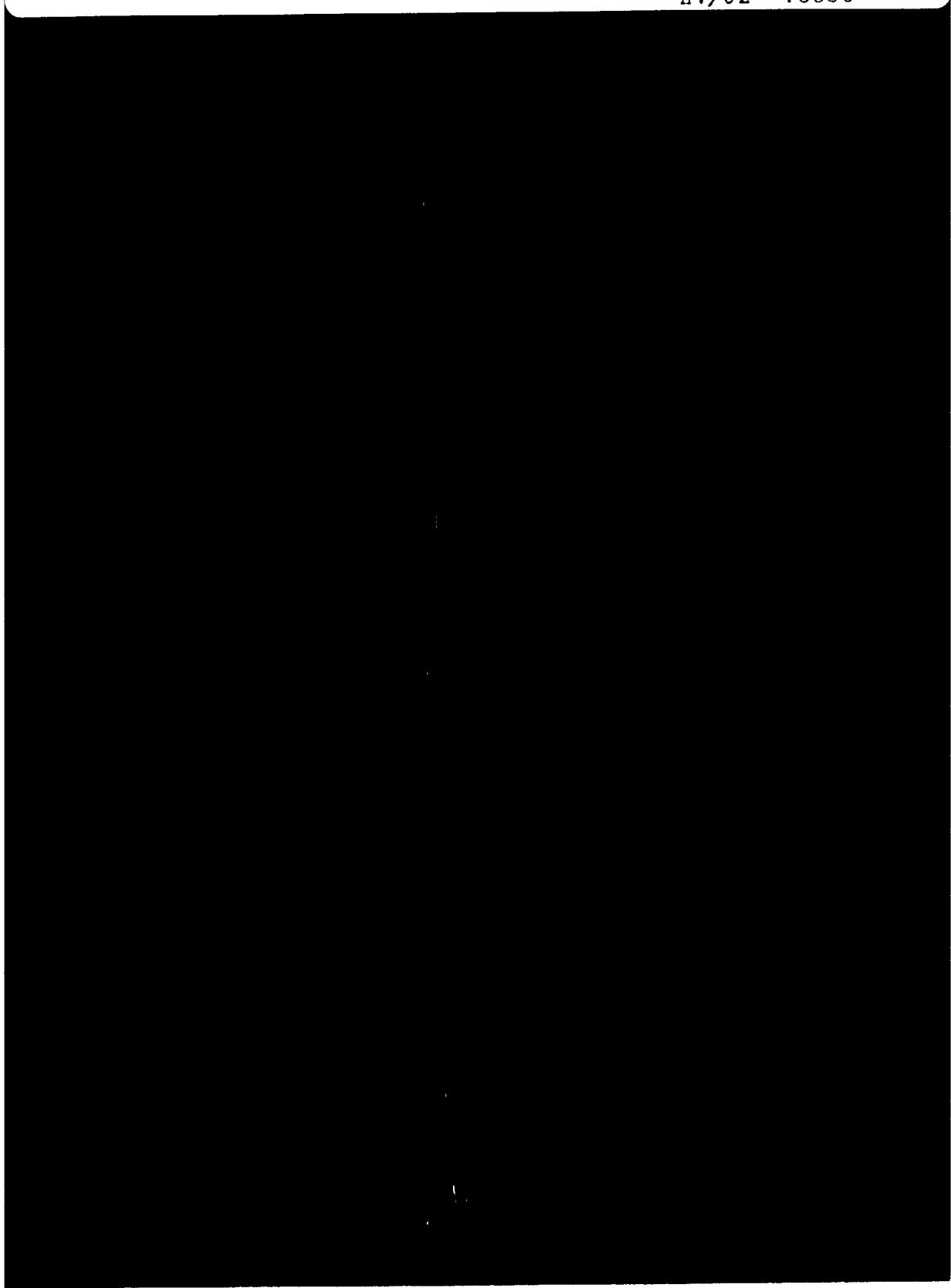


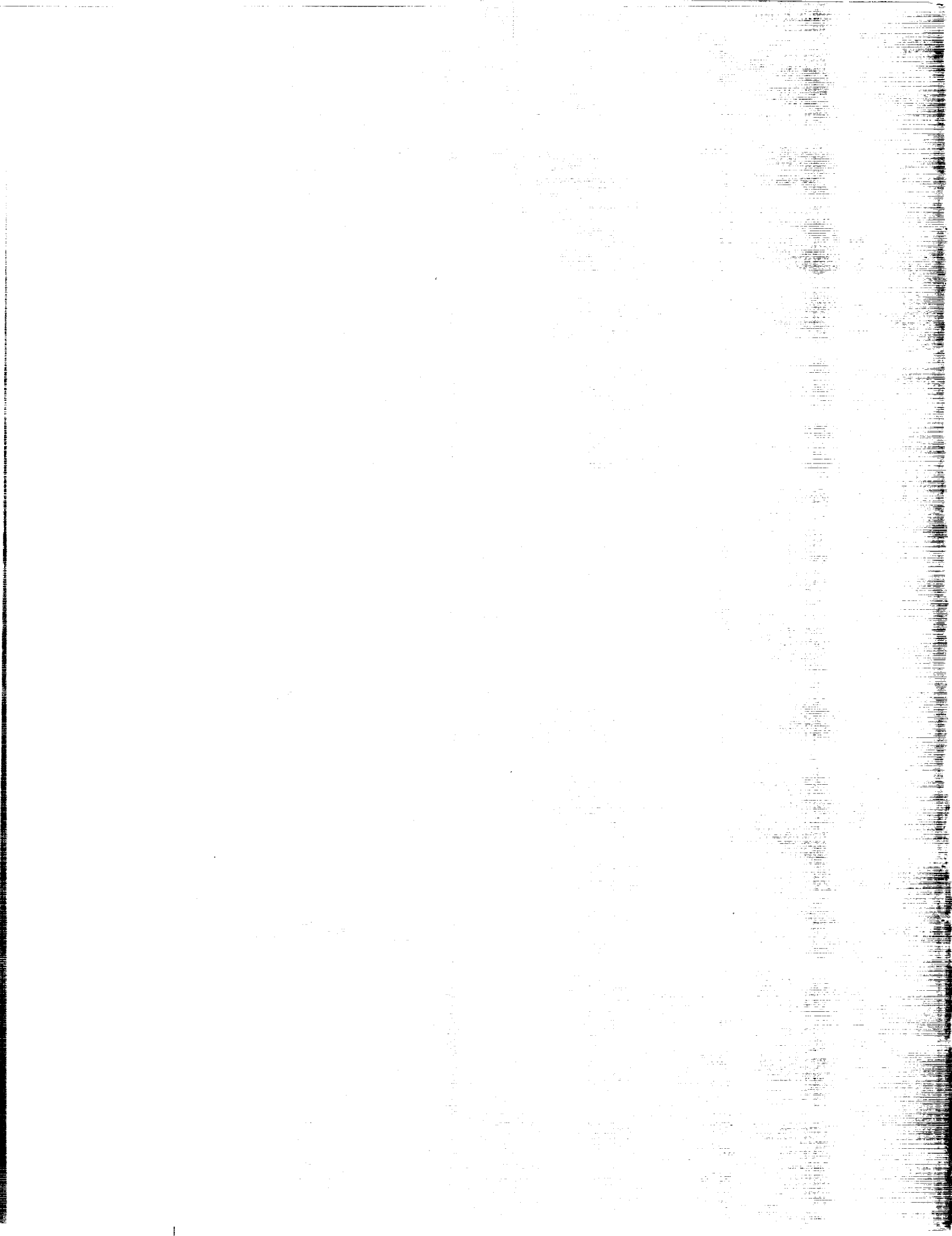
# NASA Contractor Report 3779

NUMERICAL STUDIES OF THE DEPOSITION OF  
MATERIAL RELEASED FROM FIXED AND ROTARY WING  
AIRCRAFT Final Report (Continuum Dynamics,  
Inc.) 61 p HC A04/MF A01 CSCL 01A

Unclas

H1/02 18866 Unclas





NASA Contractor Report 3779

**Numerical Studies of the  
Deposition of Material  
Released From Fixed and  
Rotary Wing Aircraft**

Alan J. Bilanin and Milton E. Teske  
*Continuum Dynamics, Inc.*  
*Princeton, New Jersey*

Prepared for  
Langley Research Center  
under Contract NAS1-16031

**NASA**  
National Aeronautics  
and Space Administration

**Scientific and Technical  
Information Office**

1984



NUMERICAL STUDIES OF THE DEPOSITION OF MATERIAL RELEASED  
FROM FIXED AND ROTARY WING AIRCRAFT

Alan J. Bilanin and Milton E. Teske  
Continuum Dynamics, Inc., Princeton, New Jersey 08540

SUMMARY

The computer code "AGDISP" (Agricultural DISpersal) has been developed to predict the deposition of material released from fixed and rotary wing aircraft in a single-pass, computationally efficient manner. The formulation of the code is novel in that the mean particle trajectory and the variance about the mean resulting from turbulent fluid fluctuations are simultaneously predicted. The code presently includes the capability of assessing the influence of neutral atmospheric conditions, inviscid wake vortices, particle evaporation, plant canopy and terrain on the deposition pattern.

The AGDISP code is appropriate for predicting the motion of material released for times over which aircraft-unique wake and propulsion system effects are still influencing the motion of the released material, and sufficient diffusion has not resulted in a distinct spray cloud. For later times Gaussian plume modeling or other methodologies may become more efficient. AGDISP output is therefore configured in a format which may be used as input to these later-time codes. The AGDISP code has an additional flexibility in allowing the user to specify a flow field independent of the flow model options available in the code. This feature gives AGDISP the capability of investigating particle dispersion in specific situations of interest.

PRECEDING PAGE BLANK NOT FILMED

## TABLE OF CONTENTS

<u>Section</u>	<u>Page</u>
SUMMARY	iii
NOMENCLATURE	v
1. INTRODUCTION	1
2. PARTICLE DYNAMIC MODELING	3
Particle Description	3
Equations Governing Particle Dynamics	3
Evaporation Model	11
3. FLOW FIELD MODELING	14
Aircraft Vortex Wake Including Wake Roll Up	14
Helicopter Flow Field	22
Propeller Swirl	26
Simple Terrain	28
Cross-Wind	28
Plant Canopy	30
Superequilibrium Turbulence	34
4. APPLICABILITY OF AGDISP FOR LONG TIME DEPOSITION STUDIES	36
5. AGDISP VALIDATION AND SAMPLE CASES	37
Helicopter with Boom Extending Outboard of a Rotor	37
Material Release in a Neutral Turbulent Atmospheric	
Boundary Layer	37
Fixed Wing Aircraft with Triangular and Rectangular	
Spanwise Load Distribution	41
Cross-Wind	45
Evaporation	45
6. AGLINE	48
7. CONCLUSIONS AND RECOMMENDATIONS	50
8. REFERENCES	51

## NOMENCLATURE

$a$	penetration depth of vortex into canopy
$A(z)$	plant areal density
$A_T$	total vortex area
$A'$	vortex area submerged within the canopy
$\bar{A}$	depth-averaged plant areal density, Eq. (71)
$b$	aircraft wing span
$\bar{b}$	vortex separation distance
$C_C$	effective canopy drag coefficient
$C_D$	particle or aircraft drag coefficient
$D$	drag of aircraft
$D_p$	particle diameter
$F_i$	particle drag force in the $i$ th direction
$g_i$	gravity
$h$	height or altitude above ground
$h_c$	canopy height
$\hat{i}, \hat{j}, \hat{k}$	unit cartesian vectors
$K$	integrated spectral density function, Eq. (24)
$\ell$	unrolled sheet length
$L$	aerodynamic lift of aircraft
$L_{TS}$	characteristic turbulent scale length, Eq. (77)
$M_p$	particle mass
$q^2$	mean square turbulence level, equal to $\langle u_1 u_1 \rangle + \langle u_2 u_2 \rangle + \langle u_3 u_3 \rangle$
$Q$	propeller torque
$r, R$	radius
$r_c$	location of the centroid of vorticity
$Re$	Reynolds number, Eq. (5)

## NOMENCLATURE (Cont'd)

S	wing planform area
T	aircraft thrust
t	time
$u_i$	fluctuating fluid velocity
$U_i$	mean fluid velocity
U	fluid velocity
$U_\infty$	aircraft flight speed
$\Delta U_1$	incremental flow velocity in the x direction
$U_*$	surface shear stress velocity
$v_i$	particle fluctuating velocity
$V_i$	particle mean velocity
$V_{rel}$	relative velocity between particle and ambient conditions, $\left  U_i + u_i - V_i - v_i \right $
W	aircraft weight
x,y,z	cartesian coordinates (x is in the direction of forward flight, y is along the wing and z is vertically upward)
$x_i$	particle fluctuating position
$X_i$	particle mean position
$x_0$	virtual origin for propeller slipstream
$z_c$	effective canopy roughness height
$z_{cr}$	centerline of skewed rotor wake
$z_d$	altitude at which the cross-wind velocity is specified
$z_0$	surface roughness
$\beta$	evaporation parameter, Eq. (36)
$\Gamma$	circulation
$\Gamma_0$	circulation at the wing centerline
$\delta_{ij}$	Kroneker delta function



## NOMENCLATURE (Cont'd)

$\zeta$	local vorticity
$\eta$	propeller efficiency
$\Delta\theta$	wet-bulb temperature depression
$\Lambda$	integral scale of turbulence
$\mu$	advance ratio
$\mu_o$	maximum advance ratio
$\nu_{\text{air}}$	kinematic viscosity of air
$\rho_{\text{air}}$	density of air
$\rho_p$	particle density
$\tau_e$	evaporation time scale, Eq. (35)
$\tau_p$	particle relaxation time scale, Eq. (7)
$\tau_T$	turbulent time scale
$\Phi_u(\omega)$	spectral density function for transverse velocity fluctuations
$\omega$	frequency
$\Omega_p$	propeller angular velocity
$\Omega_q$	propeller rotational speed
$  \quad  $	magnitude
$\langle \quad \rangle$	ensemble averaged variable
$(\vec{\quad})$	vector quantity
$( \quad )_{\text{ave}}$	average value
$( \quad )_f$	refers to flap vortex
$( \quad )_{\text{max}}$	maximum value
$( \quad )_o$	initial conditions
$( \quad )_p$	refers to propeller
$( \quad )_s$	refers to dividing streamline

NOMENCLATURE (Cont'd)

- ( )<sub>R</sub> refers to helicopter rotor
- ( )<sub>R</sub> refers to rectangularly loaded wing
- ( )<sub>t</sub> refers to tip vortex
- ( )<sub>T</sub> refers to triangularly loaded wing
- ( )<sub>1</sub> refers to the x direction
- ( )<sub>2</sub> refers to the y direction
- ( )<sub>3</sub> refers to the z direction

## 1. INTRODUCTION

The development of "AGDISP" was motivated by a desire to determine how aircraft-unique wake and propulsion system characteristics affect the ground deposition pattern of aurally released material. Development of aircraft flow field models during NASA's vortex wake hazard program provided sufficiently detailed, yet simple, models (at least for fixed wing aircraft) which could be utilized in this application. What was needed was the development of an efficient algorithm permitting the prediction of particle dynamics including the effects of turbulent fluid fluctuations. Development of this algorithm as well as a description of the flow field models programmed into the AGDISP code form the subject of this report.

Historically computers have been used since 1953 to compute the motion of material released from aircraft, with the first published study undertaken by Reed.<sup>(1)</sup> While Reed grossly oversimplified the aircraft wake flow field by neglecting roll up of the vortex sheet trailed from the wing and omitting propeller swirling wash, he did acknowledge the importance of the vortex wake in establishing particle trajectories. The model developed by him integrated the equations of motion governing the dynamics of single particles in a vortex wake flow field modeled as two counter-rotating irrotational line vortices with separation distance equal to the span of the wing. Image vortices were used to simulate an inviscid ground plane. Resultant trajectories were determined for several particle sizes released from several positions along the trailing edge of the wing; then, assuming a particle size spectrum, an expression for the deposition on the ground was developed.

The strength of the Reed model rests with its simplicity. It has been the starting point for several more recent formulations of the problem. Trayford and Welch<sup>(2)</sup> added the effects of propeller wash, cross-wind and evaporation to the Reed model. Their calculations showed that both the propeller wash and cross-wind could have a significant effect on the deposition pattern. Unfortunately, we believe that they did not include the effect of evaporation correctly in the droplet dynamic equations. When mass is lost from a droplet in relative motion with a gas, both the droplet and gas must feel opposite forces of magnitude  $V_{rel}dM_p/dt$  where  $V_{rel}$  is the relative velocity and  $dM_p/dt$  is the rate of mass lost. The Trayford and Welch model did not include this force contribution to the particle equation of motion. Additionally, as in the Reed model, the interaction of the vortices with the ground plane was assumed to be inviscid.

More recently, Bragg<sup>(3)</sup> attempted to improve the flow field in the Reed model by including the effect of bound circulation on the wing as well as allowing for some three-dimensionality in the vortex wake. Since this model was used to help guide definition of subscale deposition experiments at the Langley Vortex Research Facility, the effect of inviscid tunnel walls was also included. Recently, Loats Associates, Inc.<sup>(4)</sup> reviewed additional deposition models used to predict aerial spray drift. These additional models, in general, utilize Gaussian plume modeling and thus do not give accurate predictions when strong aircraft flow fields are influencing particle behavior.

In a series of reports, Wickens<sup>(5,6)</sup> discussed the aerodynamics of wakes from fixed wing aircraft and their implication with regard to aerial application. Wickens acknowledged that the vortex flow field and its interaction with the atmosphere and the surface is far more complicated than that which could be modeled by two inviscid point vortices. Recently, Bilanin et al.<sup>(7)</sup>, using NASA Langley's WAKE computer code, demonstrated that the viscous interaction of a vortex pair with the ground results in the shedding of secondary vorticity from the surface. This secondary vorticity completely alters the trajectories of the vortices and results in the vortices actually moving away from the surface. Jordan et al.<sup>(8)</sup>, using vortex trajectory data measured in the Langley Vortex Research Facility, compared measurements with computations of the viscous interaction of the vortex pair with the ground and found favorable agreement. Further support that complicated interactions may be expected in a canopy with and without cross shear is given in computations presented by Morris<sup>(9)</sup>. Here the descent of a vortex pair into a forest canopy was simulated, and the computation showed that the canopy would halt the lateral motion of the pair. Computations of vortex pairs in proximity to the ground with cross-wind shear produce a tipping of the pair, an observed phenomenon.

The computer code WAKE, developed by Teske<sup>(10,11)</sup>, is capable of computing the turbulent evolution of an aircraft wake flow field interacting with the atmosphere and the ground. In principle this code can provide the flow field upon which a dispersal code is based. The computer resource necessary to generate these flow field results, however, can be quite significant.

It would seem, therefore, that the largest obstacle to predicting the dispersal of material from agricultural aircraft is the determination of the flow field acting on the particles. In principle, however, the technologies required to define these turbulent flow fields are readily available. When the particle concentrations are sufficiently dilute, momentum transfer from the particle to the fluid may be neglected (the dynamics of the fluid are then uncoupled from the particle). What remains to be determined is whether the particle dispersion can be adequately described by an Eulerian or Lagrangian formulation within reasonable computational limits.

This report is organized as follows. In Section 2 the equations governing the motion of aeri ally released particles are developed, including a description of the evaporation model used. In Section 3 the flow field options available in the AGDISP code are reviewed. Code limitations and applicability are included in Section 4 and case studies form Section 5. The equivalent Gaussian distribution is discussed in Section 6. Lastly in Section 7, conclusions and recommendations are offered.

## 2. PARTICLE DYNAMIC MODELING

### Particle Description

The motion of particles may be computed from either an Eulerian or Lagrangian formulation. After analysis of computer time requirements, it was judged that the Lagrangian formulation would be far more economical, since many parametric engineering computations might ultimately result. The Eulerian or field description of a spray cloud would involve the numerical solution of partial differential equations which presently requires a large computer resource. On the other hand, a Lagrangian formulation, tracking the motion of each particle separately, requires the straightforward numerical solution of ordinary differential equations. For these reasons a Lagrangian formulation was chosen as the particle description in the AGDISP code.

### Equations Governing Particle Dynamics

The significant forces acting on aeriually released material include:

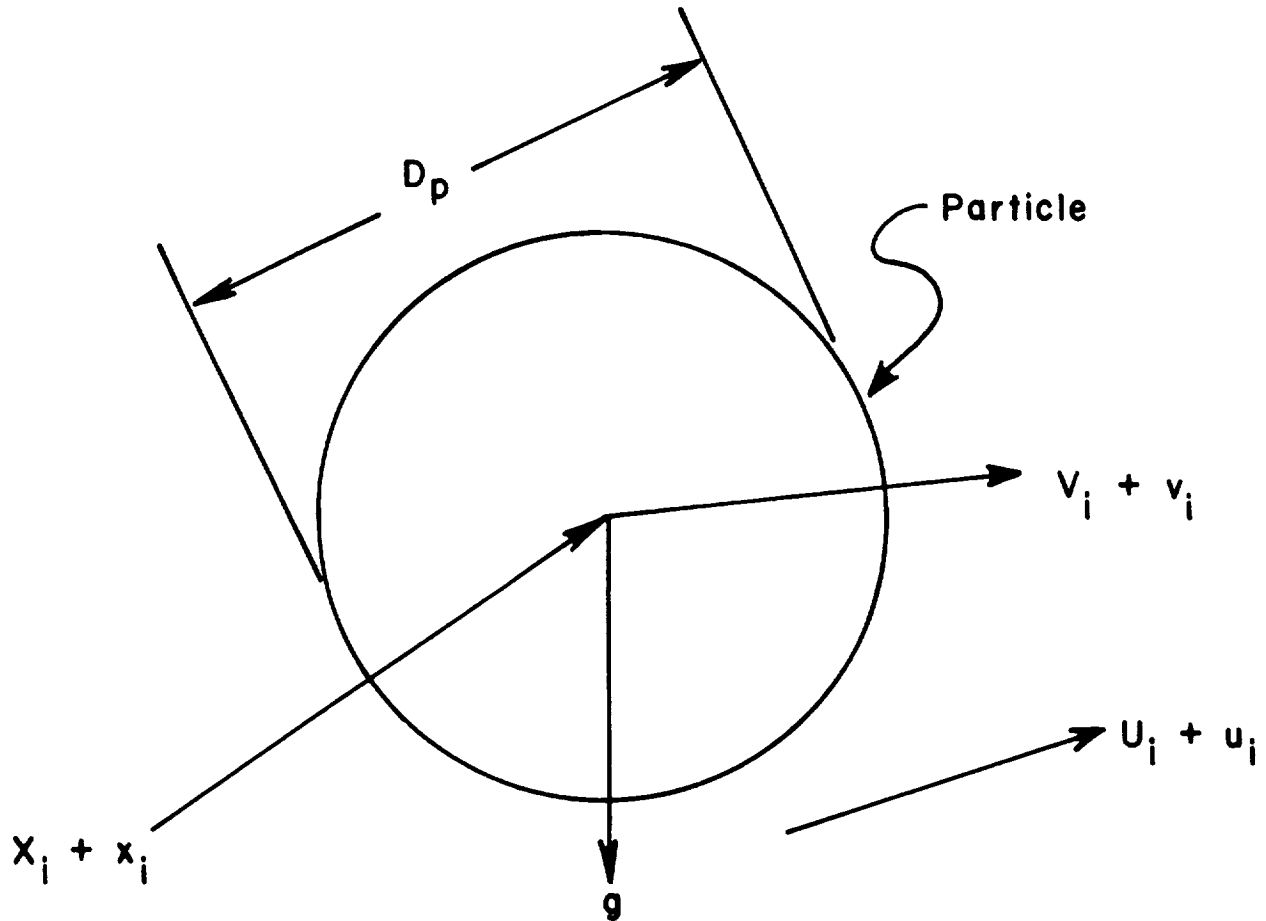
- a) Weight
- b) Aerodynamic drag
- c) Force resulting from evaporation

As shown in Figure 1, these forces result in an acceleration of a particle of mass,  $M_p$ , according to:

$$\frac{d^2}{dt^2} (X_i + x_i) = \underbrace{\frac{F_i}{M_p}}_{\text{viscous drag}} + \underbrace{\frac{(U_i + u_i - V_i - v_i)}{M_p} \frac{dM_p}{dt}}_{\text{acceleration resulting from evaporation}} + \underbrace{g_i}_{\text{gravity}} \quad (1)$$

Here,  $X_i$ ,  $V_i$  and  $U_i$  are the ensemble averaged  $i^{\text{th}}$  component of particle position, velocity and fluid velocity, respectively, while  $x_i$ ,  $v_i$  and  $u_i$  are the fluctuating  $i^{\text{th}}$  component of particle position, velocity and fluid velocity, respectively. The particle velocity is related to the particle position through:

$$\frac{d(X_i + x_i)}{dt} = V_i + v_i \quad (2)$$



$X_i, V_i, U_i - i^{\text{th}}$  ensemble averaged component of particle position, velocity and fluid velocity, respectively.

$x_i, v_i, u_i - i^{\text{th}}$  fluctuating component of particle position, velocity and fluid velocity, respectively.

Figure 1. Particle notation convention

The drag force on the particle is computed from:

$$\frac{F_i}{M_p} = \frac{3}{4} \frac{C_D \rho_{air}}{D_p \rho_p} \left| U_i + u_i - V_i - v_i \right| (U_i + u_i - V_i - v_i) \quad (3)$$

where  $C_D$  is the Reynolds number dependent drag coefficient of the assumed spherical particle of diameter  $D_p$  and density  $\rho_p$ , and  $\rho_{air}$  is the density of air.

Currently, we are using a semi-empirical relationship for  $C_D$  suggested by Langmuir and Blodgett<sup>(12)</sup>:

$$C_D = \frac{24}{Re} (1 + 0.197Re^{0.63} + 2.6 \times 10^{-4} Re^{1.38}) \quad (4)$$

where  $Re$  is the Reynolds number defined as:

$$Re = \frac{D_p V_{rel}}{\nu_{air}} \quad (5)$$

Equation (4) is valid for spherical particles in the range  $0 < Re < 50000$ .<sup>(12)</sup> Substituting for  $C_D$  in Eq. (3) yields:

$$\frac{F_i}{M_p} = \frac{1}{\tau_p} (U_i + u_i - V_i - v_i) \quad (6)$$

where  $\tau_p$  is the particle relaxation time computed from:

$$\tau_p = \frac{D_p^2 \rho_p}{18 \nu_{air} \rho_{air}} \left( 1 + 0.197Re^{0.63} + 2.6 \times 10^{-4} Re^{1.38} \right)^{-1} \quad (7)$$

The particle relaxation time given in Eq. (7) has physical significance with regard to dispersion in that it is a measure of the time required for a particle to catch up to the local fluid velocity. Specifically, if a particle were released at rest in a stream of velocity  $|U|$ , the time required for the particle to reach  $0.63|U|$  is  $\tau_p$ .

If Eq. (1) and Eq. (2) are ensemble averaged with the drag model from Eq. (6) and fluctuations in the evaporation rate are ignored, there results:

$$\frac{d^2 X_i}{dt^2} = (U_i - v_i) \left[ \frac{1}{\tau_p} + \frac{1}{M_p} \frac{dM_p}{dt} \right] + g_i \quad (8)$$

$$\frac{dX_i}{dt} = v_i \quad (9)$$

Subtracting Eq. (8) from Eq. (1) and Eq. (9) from Eq. (2) results in equations for the fluctuations:

$$\frac{d^2 x_i}{dt^2} = (u_i - v_i) \left[ \frac{1}{\tau_p} + \frac{1}{M_p} \frac{dM_p}{dt} \right] \quad (10)$$

$$\frac{dx_i}{dt} = v_i \quad (11)$$

which may be premultiplied by  $x_i$  and  $v_i$ , ensemble averaged and manipulated to yield:

$$\frac{d}{dt} \langle x_i x_i \rangle = 2 \langle x_i v_i \rangle \quad (12)$$

$$\frac{d}{dt} \langle x_i v_i \rangle = (\langle x_i u_i \rangle - \langle x_i v_i \rangle) \left[ \frac{1}{\tau_p} + \frac{1}{M_p} \frac{dM_p}{dt} \right] + \langle v_i v_i \rangle \quad (13)$$

$$\frac{d}{dt} \langle v_i v_i \rangle = 2(\langle u_i v_i \rangle - \langle v_i v_i \rangle) \left[ \frac{1}{\tau_p} + \frac{1}{M_p} \frac{dM_p}{dt} \right] \quad (14)$$



where no summation is implied. The symbol  $\langle \rangle$  denotes the ensemble average of the quantity.

Equations (12), (13) and (14) are nine equations for the fifteen variables  $\langle x_i v_i \rangle$ ,  $\langle v_i v_i \rangle$ ,  $\langle x_i x_i \rangle$ ,  $\langle x_i u_i \rangle$  and  $\langle u_i v_i \rangle$ . Closure is completed by specifying approximate relationships for the quantities  $\langle x_i u_i \rangle$  and  $\langle u_i v_i \rangle$ , the correlations of the particle position and velocity fluctuations, respectively, with the mean velocity fluctuation.

These relationships are developed by assuming the fluctuating fluid velocity is given by:

$$u_i(t) = \frac{1}{2\pi} \int_{-\infty}^{\infty} u_i(\omega) e^{i\omega t} d\omega \quad (15)$$

and solving

$$\frac{dv_i}{dt} = \frac{(u_i - v_i)}{\tau_p}, \quad \frac{dx_i}{dt} = v_i \quad (16)$$

for  $v_i$  and  $x_i$ , then forming the products  $x_i u_i$  and  $u_i v_i$  and ensemble averaging. With zero initial conditions, Eqs. (15) and (16) yield:

$$x_i = \frac{1}{2\pi} \int_{-\infty}^{\infty} u_i(\omega) d\omega \left\{ \frac{e^{i\omega t} - 1 + i\omega\tau_p (e^{-t/\tau_p} - 1)}{i\omega(1 + i\omega\tau_p)} \right\} \quad (17)$$

$$v_i = \frac{1}{2\pi} \int_{-\infty}^{\infty} u_i(\omega) d\omega \left\{ \frac{e^{i\omega t} - e^{-t/\tau_p}}{1 + i\omega\tau_p} \right\} \quad (18)$$

Upon multiplying Eq. (17) and Eq. (18) by  $u_i$  and ensemble averaging, we obtain:

$$\langle x_i u_i \rangle = \int_0^{\infty} \phi_u(\omega) \left\{ \frac{\sin \omega t}{\omega} - \frac{\tau_p e^{-t/\tau_p}}{1 + \tau_p^2 \omega^2} \right. \\ \left. (e^{t/\tau_p} + \tau_p \omega \sin \omega t - \cos \omega t) \right\} d\omega \quad (19)$$

and

$$\langle u_i v_i \rangle = \int_{-\infty}^{\infty} \left\{ \begin{aligned} &\phi_u(\omega) \left[ 1 - e^{-t/\tau_p} \cos \omega t \right. \\ &\left. - e^{-t/\tau_p} \tau_p \omega \sin \omega t \right] d\omega \end{aligned} \right. \quad (20)$$

where  $\phi_u(\omega)$  is the spectral density function for transverse velocity fluctuations. The spectral density function will be selected so that Eqs. (19) and (20) can be integrated and simple closure achieved.

Von Karman and Howarth<sup>(13)</sup> showed for isotropic turbulence that fluctuations normal to the mean flow may be expressed as:

$$\phi_u(\omega) = \frac{1}{3\pi} \frac{\Lambda}{U} q^2 \frac{1 + 3(\omega\Lambda/U)^2}{[1 + (\omega\Lambda/U)^2]^2} \quad (21)$$

where  $\Lambda$  is the integral scale of the turbulence,  $q^2$  is the mean square turbulence level and  $U$  is the free stream velocity. If  $U$  were now interpreted as the relative mean velocity between the aeriially released material and the mean fluid velocity, this form of  $\phi_u(\omega)$  permits an analytical evaluation of  $\langle x_i u_i \rangle$  and  $\langle u_i v_i \rangle$ . Implicit in this substitution is the assumption that the aeriially released particle is acted upon by a locally isotropic turbulent field (this assumption is compatible with the simple flow field models developed in the next section). Integration of Eqs. (19) and (20) with the assumed form of  $\phi_u(\omega)$  given in Eq. (21) yields:

$$\langle x_i u_i \rangle = \frac{q^2}{3} \left[ -\tau_p K + \frac{\tau_p}{2} \right] \quad (22)$$

$$\langle u_i v_i \rangle = \frac{q^2}{3} K \quad (23)$$

with

$$K = \frac{1}{2} \frac{\left[ 3 - \left( \frac{\tau_p}{\tau_\tau} \right)^2 \right] \left[ 1 - \frac{\tau_p}{\tau_\tau} \right] + \left( \frac{\tau_p}{\tau_\tau} \right)^2 - 1}{\left[ 1 - \left( \frac{\tau_p}{\tau_\tau} \right)^2 \right]^2} \quad (24)$$

where  $\tau_\tau = \Lambda / |V_{rel}|$  and is the time of travel of the material through the turbulent eddy of scale  $\Lambda$ . When the particle adjustment time  $\tau_p \ll \tau_\tau$ , the particle tracks the fluid motion and:

$$\langle x_i u_i \rangle = \frac{\tau_\tau q^2}{6} \quad (25)$$

$$\langle u_i v_i \rangle = \frac{q^2}{3} \quad (26)$$

Assuming that ensemble averaged fluid velocities are known and fluid fluctuating variances are prescribed, the formulation of the particle dispersal dynamics problem is complete once initial conditions are specified at  $t = 0$ .

Typically:

$$\begin{aligned} X_i &= X_{i0} \\ V_i &= V_{i0} \\ \langle x_i x_i \rangle &= \langle x_i v_i \rangle = 0 \\ \langle v_i v_i \rangle &= \langle v_i v_i \rangle_0 \end{aligned} \quad (27)$$

A non-zero specification of  $\langle v_i v_i \rangle$  allows for variance in the initial particle/droplet velocities at the point of release. The above equations are programmed in the AGDISP computer code.

To verify that the formulation of the equations governing particle displacement variance is correct, we assume that the particle has zero mass and as a result passively follows the fluid fluctuations. Then  $\tau_p \rightarrow 0$  and we may determine  $\langle x_i x_i \rangle$  for time  $t > \tau_\tau$ . Neglecting evaporation, Eqs. (14) and (26) yield:

$$\langle v_i v_i \rangle = \langle u_i v_i \rangle = \frac{q^2}{3} \quad (28)$$

Substituting this result in Eq. (13), using Eq. (25), yields:

$$\frac{d}{dt} \langle x_i v_i \rangle = \frac{1}{\tau_p} \left( \frac{\tau_\tau q^2}{6} - \langle x_i v_i \rangle \right) + \frac{q^2}{3} \quad (29)$$

which for large  $t$  may be solved to give:

$$\langle x_i v_i \rangle = \frac{\tau_\tau q^2}{6} \quad (30)$$

Therefore, from Eq. (12) we obtain:

$$\langle x_i x_i \rangle = \frac{\tau_\tau q^2 t}{3} \quad (31)$$

This result may be compared with the result obtained using second-order closure turbulent modeling for a passive tracer<sup>(14)</sup> in the  $t > \tau_\tau$  limit:

$$\langle x_i x_i \rangle = \frac{8}{9} q \Lambda t \quad (32)$$

Hence, when there is no relative ensemble average velocity between the particle and the fluid,  $\tau_\tau$  must reduce to  $8\Lambda/3q$ . Therefore, the turbulent time scale  $\tau_\tau$  must be redefined to be:

$$\tau_\tau = \frac{\Lambda}{(|v_{rel}| + \frac{3}{8} q)} \quad (33)$$

## Evaporation Model

The force on a particle as a consequence of evaporation results from the evaporating fluid leaving the droplet at a velocity  $V_i + v_i$  which is not in general equal to the local fluid velocity  $U_i + u_i$ ; hence, a momentum exchange occurs. For the present a simple evaporation model<sup>(2)</sup> is assumed:

$$\frac{1}{M_p} \frac{dM_p}{dt} = \frac{3}{2\tau_e \left(1 - \frac{t}{\tau_e}\right)} \quad (34)$$

where  $\tau_e$  is the life of the droplet and is given by:

$$\tau_e = \frac{D_p^2}{\beta \Delta\theta} \Bigg|_{t=0} \quad (35)$$

where  $\Delta\theta$  is the wet bulb depression and  $\beta$  is defined as:

$$\beta = 84.76 [1.0 + 0.27 \text{Re}^{1/2}] \quad (36)$$

in units of  $\text{m}^2/\text{sec} - ^\circ\text{C}$ .

During computation a particle is permitted to evaporate to a specified minimum particle diameter, at which point the particle diameter is held constant for the remainder of the computation. The minimum particle diameter is determined by estimating the point at which sufficient solvent has evaporated so that evaporation is inhibited by the high concentration of solute.

Recently, Dennison and Wedding<sup>(15)</sup> have conducted evaporation experiments at Colorado State University. A number of pesticides were held in a water solvent in a wind tunnel at terminal velocity using a very thin wire which spanned the tunnel. The current evaporation model was checked against this data. Predictions of droplet diameters versus elapsed time for the initial droplet size of 110 and 400  $\mu\text{m}$  are shown in Figures 2 and 3, respectively. Solution 12 is pure water. The test data and simulation were undertaken at a nominal air temperature and relative humidity of 20 deg C and 20%, respectively. This corresponds to a wet bulb depression of about 10.7 deg C. As can be seen the predictions of particle diameter are in favorable agreement with test data.

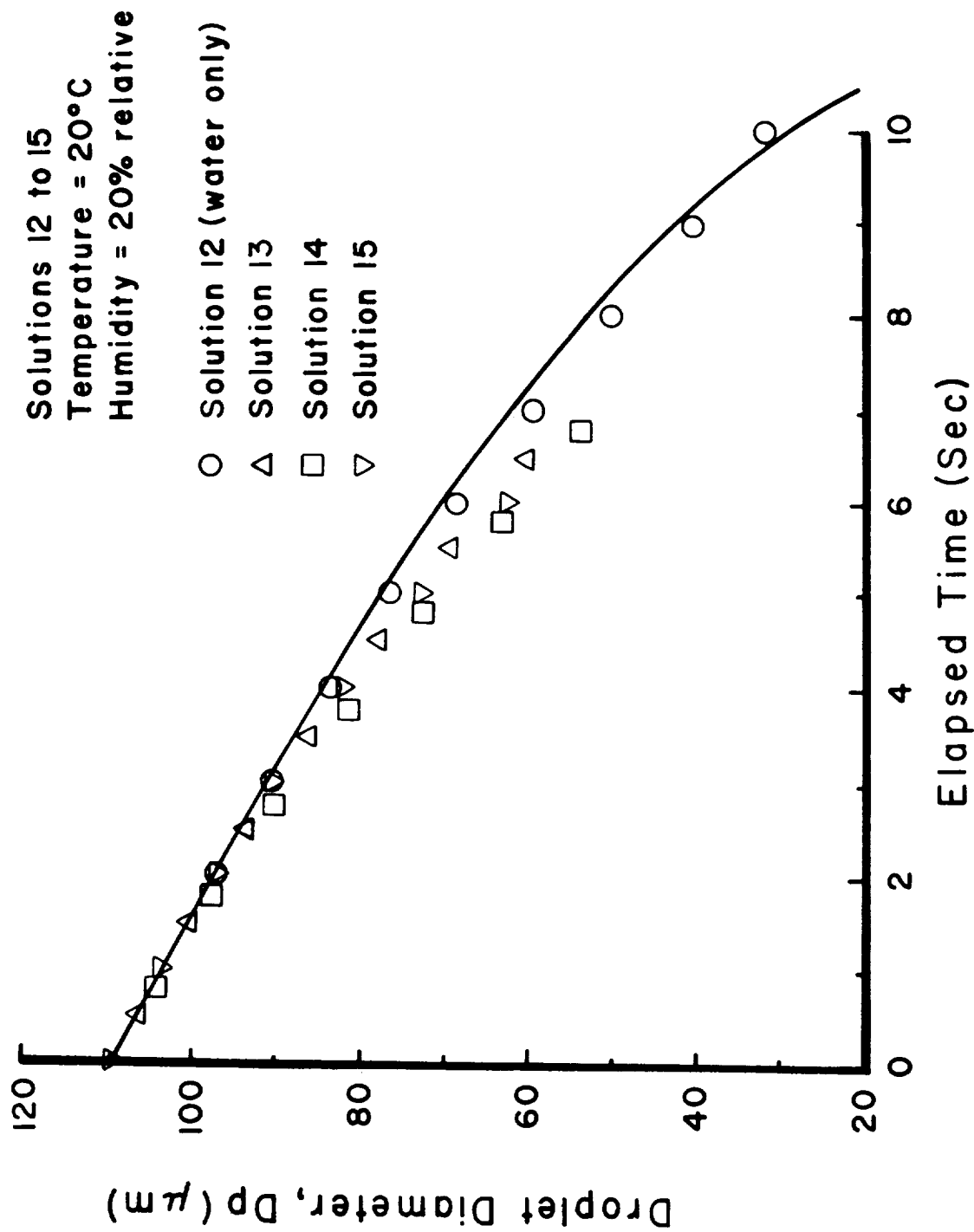


Figure 2. Prediction and measurement of droplet diameter variation with time as a consequence of evaporation

ORIGINAL PAGE IS  
OF POOR QUALITY

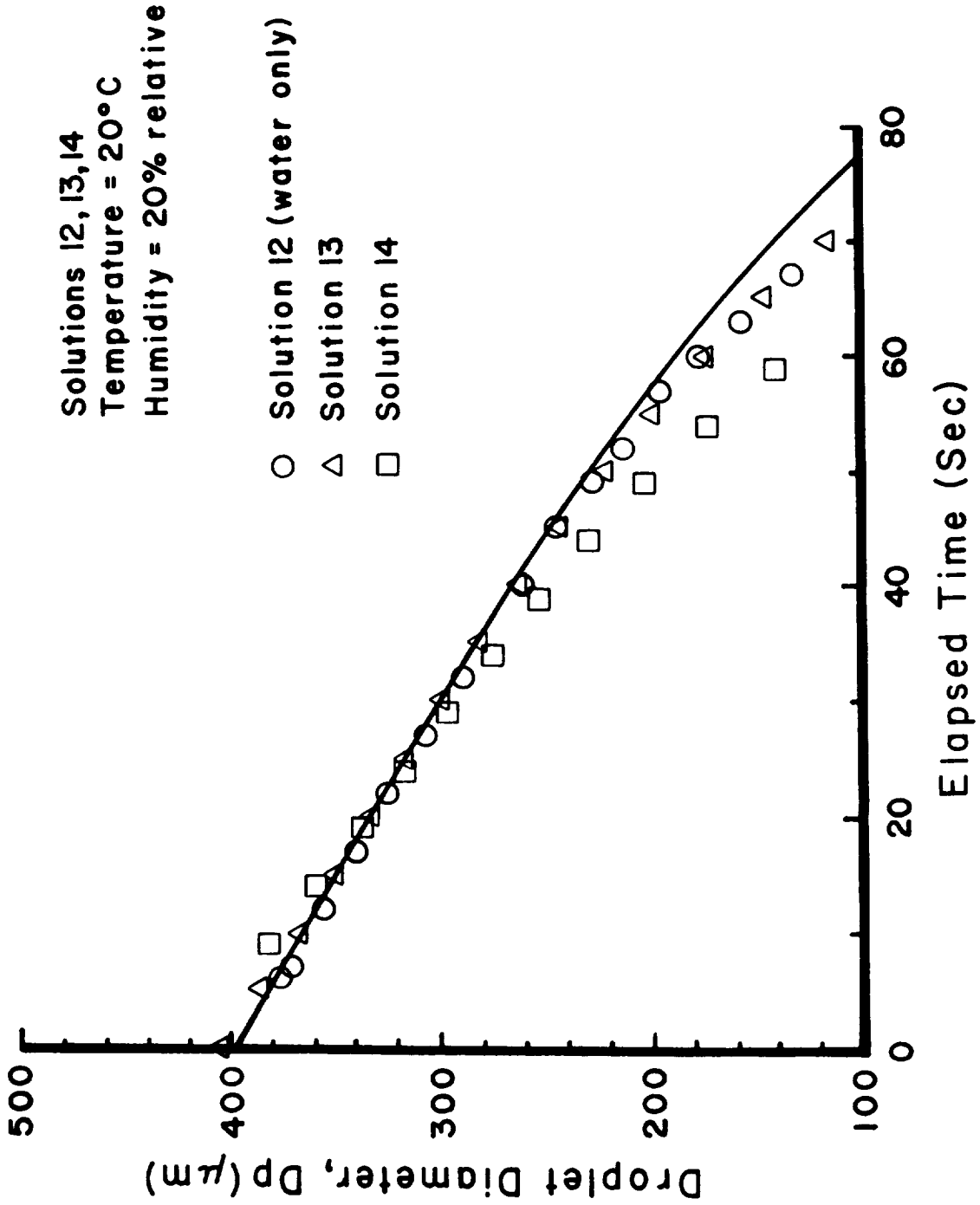


Figure 3. Prediction and measurement of droplet diameter variation with time as a consequence of evaporation

### 3. FLOW FIELD MODELING

The AGDISP code has been configured to accept user-specified mean velocity and turbulence flow fields in neutral atmospheres. Input file format requirements are detailed in the AGDISP user manual<sup>(16)</sup>. For users not wishing to supply their own flow field, the following models have been incorporated into the AGDISP code.

- 1) Aircraft vortex wake including wake roll up
- 2) Helicopter flow field
- 3) Propeller swirl
- 4) Simple terrain
- 5) Cross-wind
- 6) Plant canopy
- 7) Superequilibrium turbulence

The remainder of this chapter discusses these models.

#### Aircraft Vortex Wake Including Wake Roll Up

It is well known that fixed wing aircraft trail vortex wakes as a consequence of the aerodynamic lift generated by the wing. This wake flow field can significantly influence the dynamics of material released into it. For this reason it is important to have available in the AGDISP code a flow field model which reasonably represents the velocity field in the vortex wake of an aircraft releasing agricultural material. Fortunately, recent research sponsored primarily by NASA has resulted in an understanding of the aerodynamics of vortex wakes (the interested reader may refer to Ref. 17 for a more complete discussion of this subject). The following discussion highlights the necessary details required to understand the flow field description implemented in the AGDISP code.

When an aircraft flies at constant altitude, the aerodynamic lift,  $L$ , generated by the lifting surfaces of the aircraft equals the aircraft weight,  $W$ . Since the majority of the lift is carried by the wings and not by the tail, it is common practice to neglect the contribution to the wake of the tail aerodynamics. The wing lift distribution generates one or more pairs of swirling masses of air downstream of the aircraft (see Figure 4). These swirling masses are known as vortices. The strength of a vortex is denoted by the circulation  $\Gamma$ , and is related to the lift by:

$$L = \rho_{\text{air}} U_{\infty} \bar{b} \Gamma \quad (37)$$



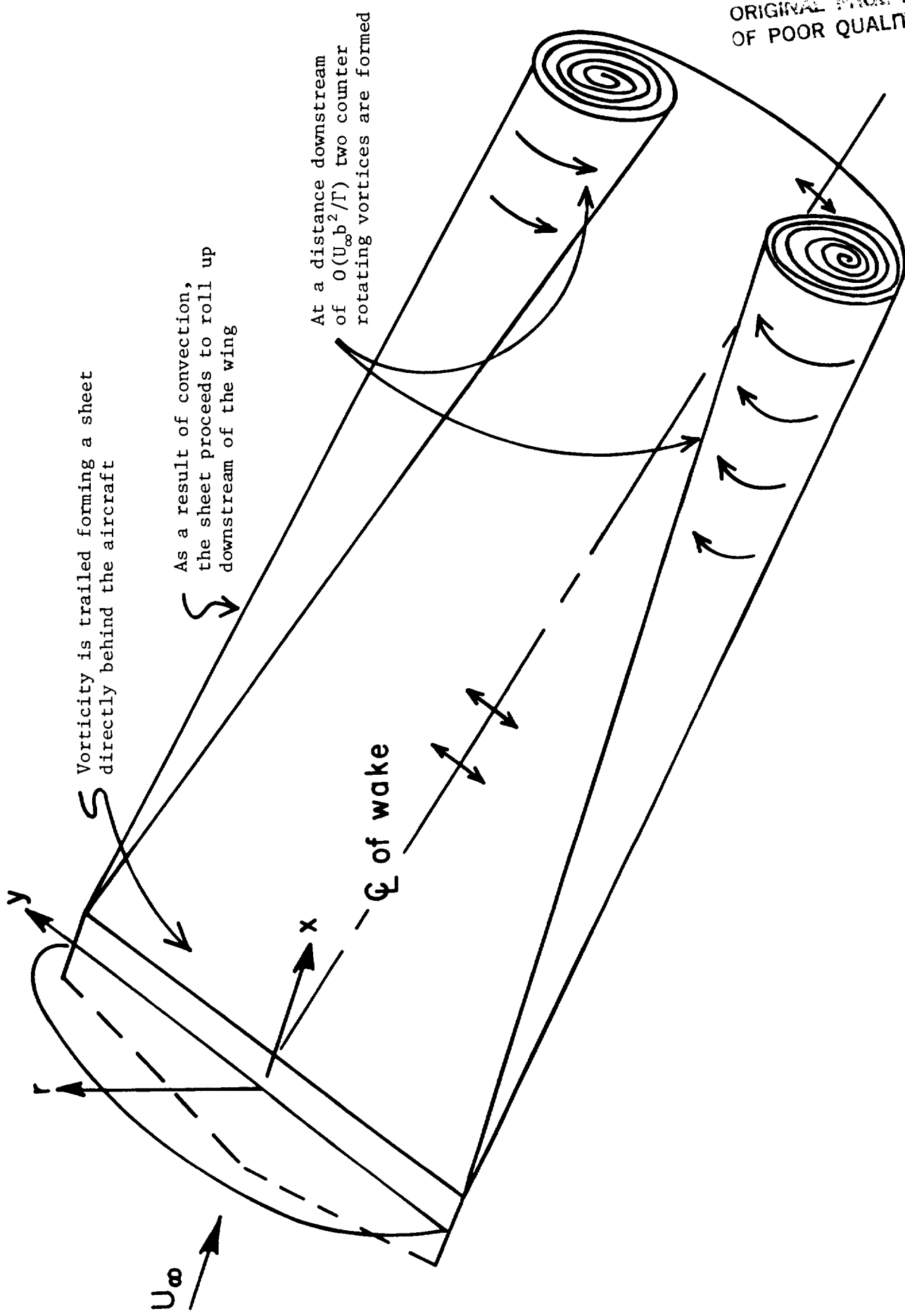


Figure 4. A schematic of the roll up of a vortex sheet trailed from a simply loaded wing

where  $U_\infty$  and  $\bar{b}$  are the flight speed of the aircraft and separation between the vortices, respectively. Unfortunately, the vortex wake immediately behind the aircraft (as shown in Figure 4) is generally much more complicated since the wake is in fact a thin sheet of vorticity trailed from the wing. This sheet rolls up downstream into discrete vortex pairs. The wake shown in Figure 4 is for a simply loaded wing; that is, a wing with a load distribution which trails a sheet of vorticity that will roll up into one pair of counter-rotating vortices. The wake flow field resulting from a lifting wing will become more complicated when this simple load distribution is altered by a deployed flap, as shown in Figure 5. In this case, in the far wake, two vortex pairs eventually roll up and descend under their mutual influence.

In the AGDISP code the far field swirling velocities in the vortices are estimated using an approximate methodology first suggested by Betz.<sup>(18)</sup> This methodology relates the swirling velocity distribution in the vortices to the details of the wing spanwise load distribution by assuming that angular momentum is approximately conserved. Figure 6 shows the swirling velocity distribution which results after roll up is complete behind wings that have spanwise load distributions that are triangular, elliptical and rectangular. The details of how these swirling velocities are computed from the spanwise load distribution is documented in Ref. 19.

The above discussion presumes that the aircraft is at a sufficiently high altitude such that wake interaction with the ground may be neglected. Under most conditions of interest with regard to aerial application, however, this is not a good approximation and the influence of the ground must be included. To first order the most significant effect of the ground is to force the vertical component of fluid velocity to be zero at the surface.

Out of ground influence, the vortex pair descends downward with a velocity of  $\Gamma/2\pi\bar{b}$  while maintaining a constant separation distance between the vortices. The most important near ground effect is to force vortex motion along the surface as shown schematically in Figure 7. This effect of the ground plane on vortex motion is included in the AGDISP code.

Since all agricultural material must for practical reasons be released in the immediate vicinity of the aircraft, the wake flow field model must be extended, if sufficient predictive accuracy demands it, to properly account for the unrolled portion of the aircraft wake. The details of treating sheet roll up into discrete vortices is documented in Ref. 19. Here we will highlight the general features of the Betz roll up model included in the AGDISP code.

Figure 5 illustrates the roll up of a tip and interior flap vortex. The vortical material trailed from the trailing edge of the wing makes up a sheet which is convected about the local concentrations of vorticity. These local concentrations are located spanwise at positions where the slope of the wing spanwise load distribution is a local maximum (in practice these positions occur where edges of flaps or spoilers are located). Downstream of the wing, the AGDISP code rolls up the trailed vorticity in a manner analogous to the roll up of a window shade. The strength of the vortex increases as additional vorticity is brought into the rolled up vortex at velocity  $U_t(t) = \Gamma_t/2\pi R_t(t)$  for a tip vortex. The circulation increases according to:

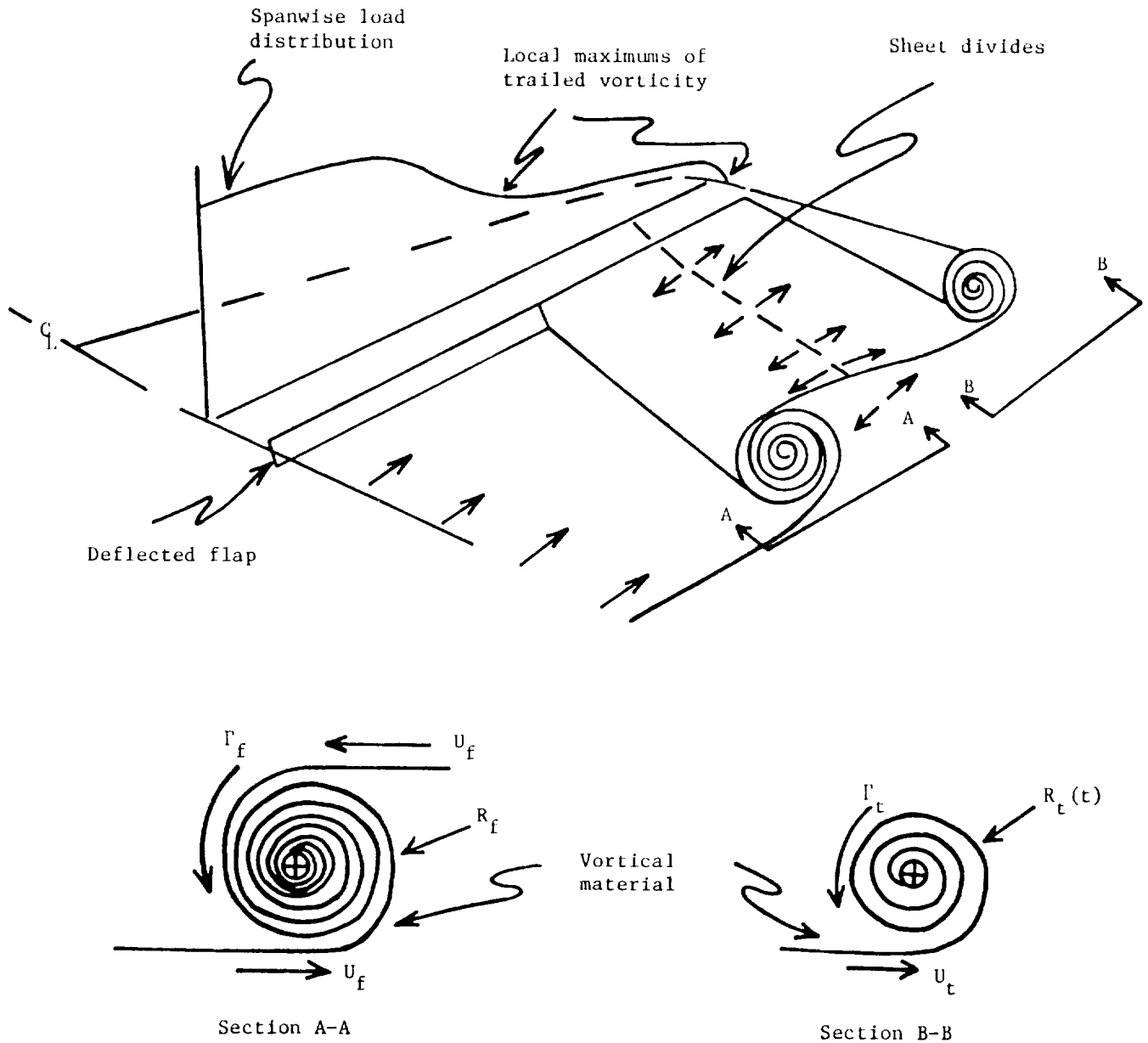


Figure 5. Schematic of the roll up of a tip and interior vortex

ORIGINAL PAGE IS  
OF POOR QUALITY

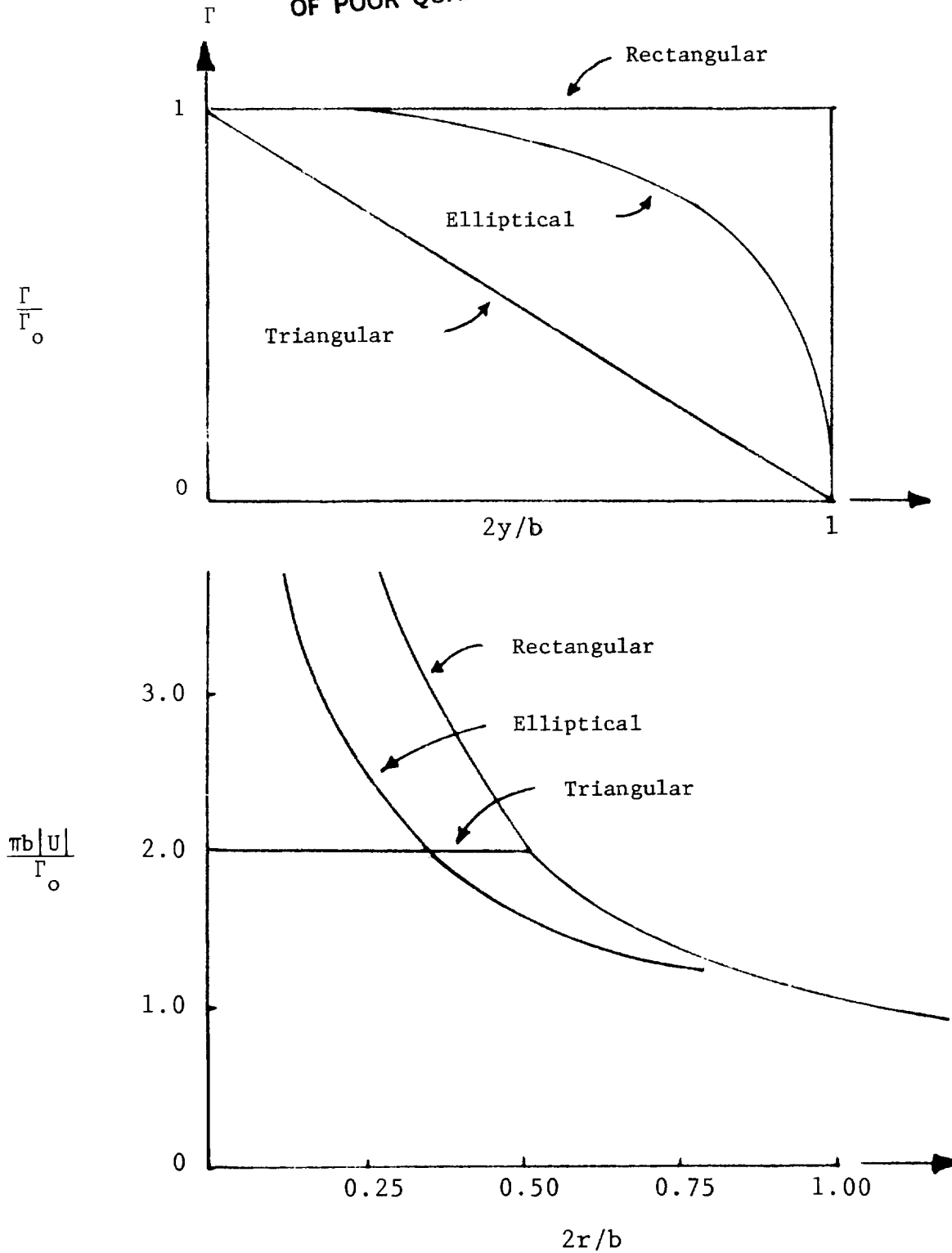


Figure 6. Swirl velocity distribution of a fully rolled up wake as a function of spanwise lift distribution and as measured from the center of the resulting vortex

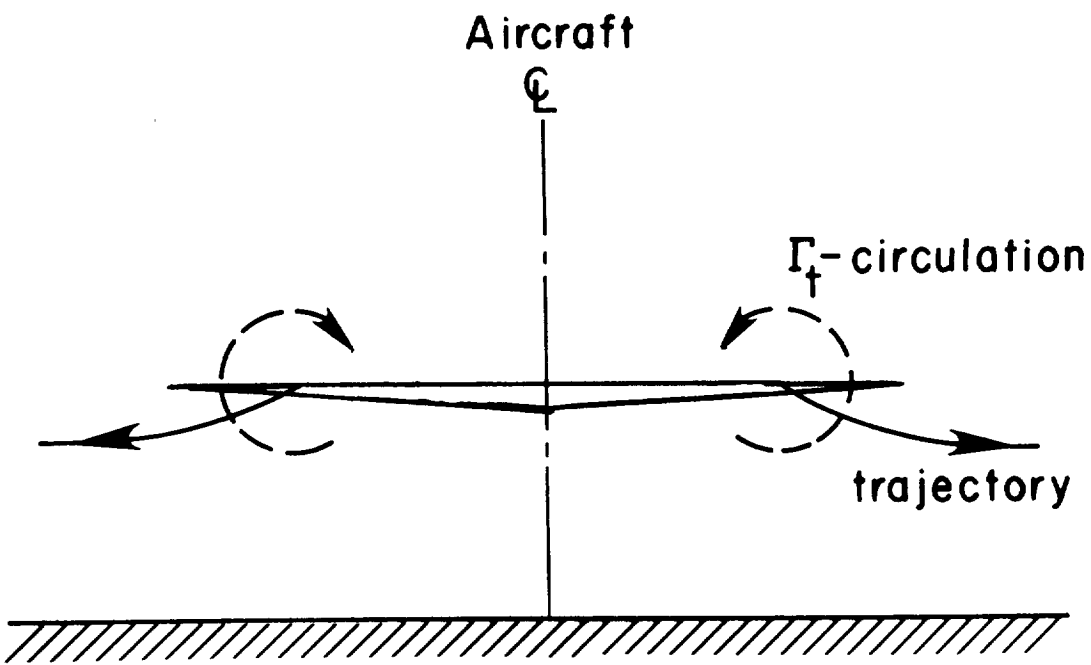
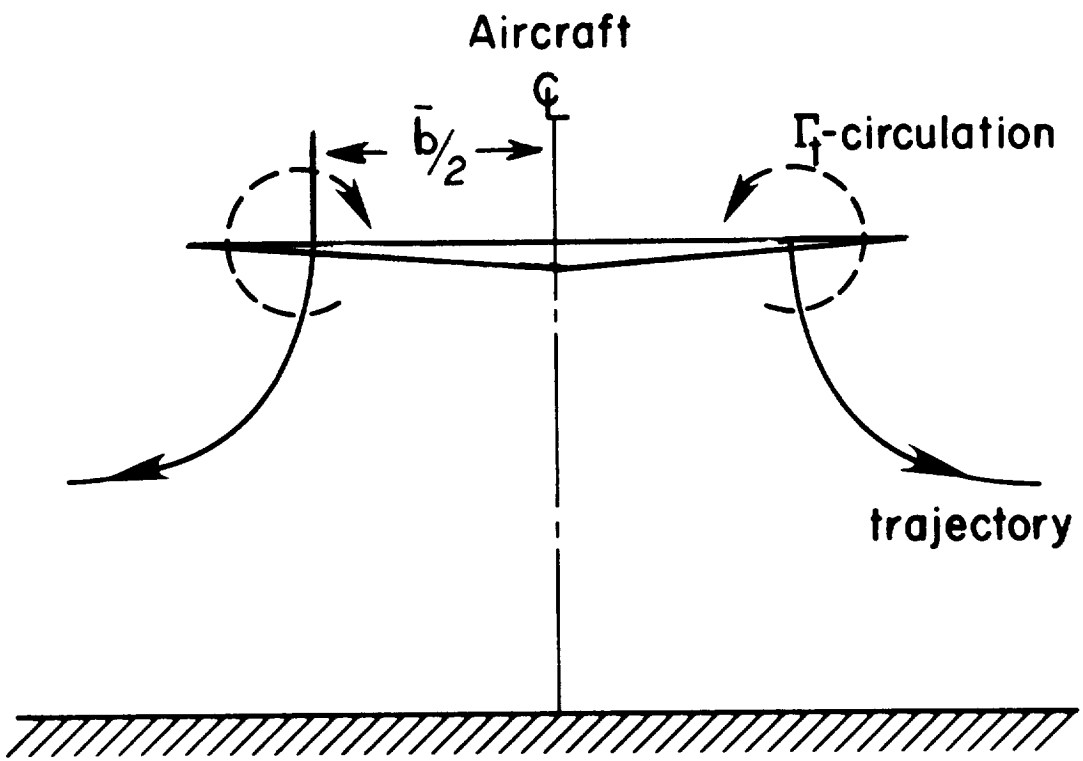


Figure 7. Trajectories of a vortex pair approaching the ground

$$\frac{d\Gamma_t}{dt} = -\frac{\Gamma_t}{2\pi R_t} \frac{d\Gamma}{dy} \quad (38)$$

where  $d\Gamma/dy$  is the strength of the vortex sheet rolling into the vortex and  $R_t(t)$  is the Betz vortex radius computed as described in Ref. 19.

While the vortices roll up, they are also in motion relative to each other. It may be shown that for two-dimensional vortices the motion of the centroid of a vortex is given by:

$$\frac{d\vec{r}_c}{dt} = \int \frac{(U_s \hat{j} + U_3 \hat{k}) \zeta}{\Gamma} dydz \quad (39)$$

where the centroid is defined as:

$$\vec{r}_c = \int \frac{(y \hat{j} + z \hat{k}) \zeta}{\Gamma} dydz \quad (40)$$

and  $\zeta$  is the vorticity. The velocity components  $U_2$  and  $U_3$  are the velocities resulting from all additional concentrations of vorticity excluding the centroid under consideration. During the evolution of the wake flow field, the AGDISP code tracks the position of the discrete concentrations of vorticity by integrating Eq. (39).

The velocity field generated by the roll up process may be obtained once the location of the discrete concentrations of vorticity and the strength remaining in the unrolled sheets are known. Figure 8 illustrates this process. The velocity field at position "A" results from eight contributions: the right and left partially rolled up vortices, the right and left unrolled up sheets, and their image vortices and sheets. The velocity contribution from the right unrolled up sheet is computed from:

$$\begin{aligned} \vec{U}(x) = \frac{\Gamma_{ave}}{8\pi\ell} & \left\{ \hat{k} \ell n \frac{r_+^2 [\sqrt{r_+^2 + x^2} - x] [\sqrt{r_-^2 + x^2} + x]}{r_-^2 [\sqrt{r_+^2 + x^2} + x] [\sqrt{r_-^2 + x^2} - x]} \right. \\ & - 2\hat{j} \tan^{-1} \left[ \left( \frac{\ell - y}{z} \right) + \tan^{-1} \left( \frac{y}{z} \right) \right. \\ & \left. \left. + \tan^{-1} \left( \frac{x(\ell - y)}{z\sqrt{r_-^2 + x^2}} \right) + \tan^{-1} \left( \frac{xy}{z\sqrt{r_+^2 + x^2}} \right) \right] \right\} \quad (41) \end{aligned}$$

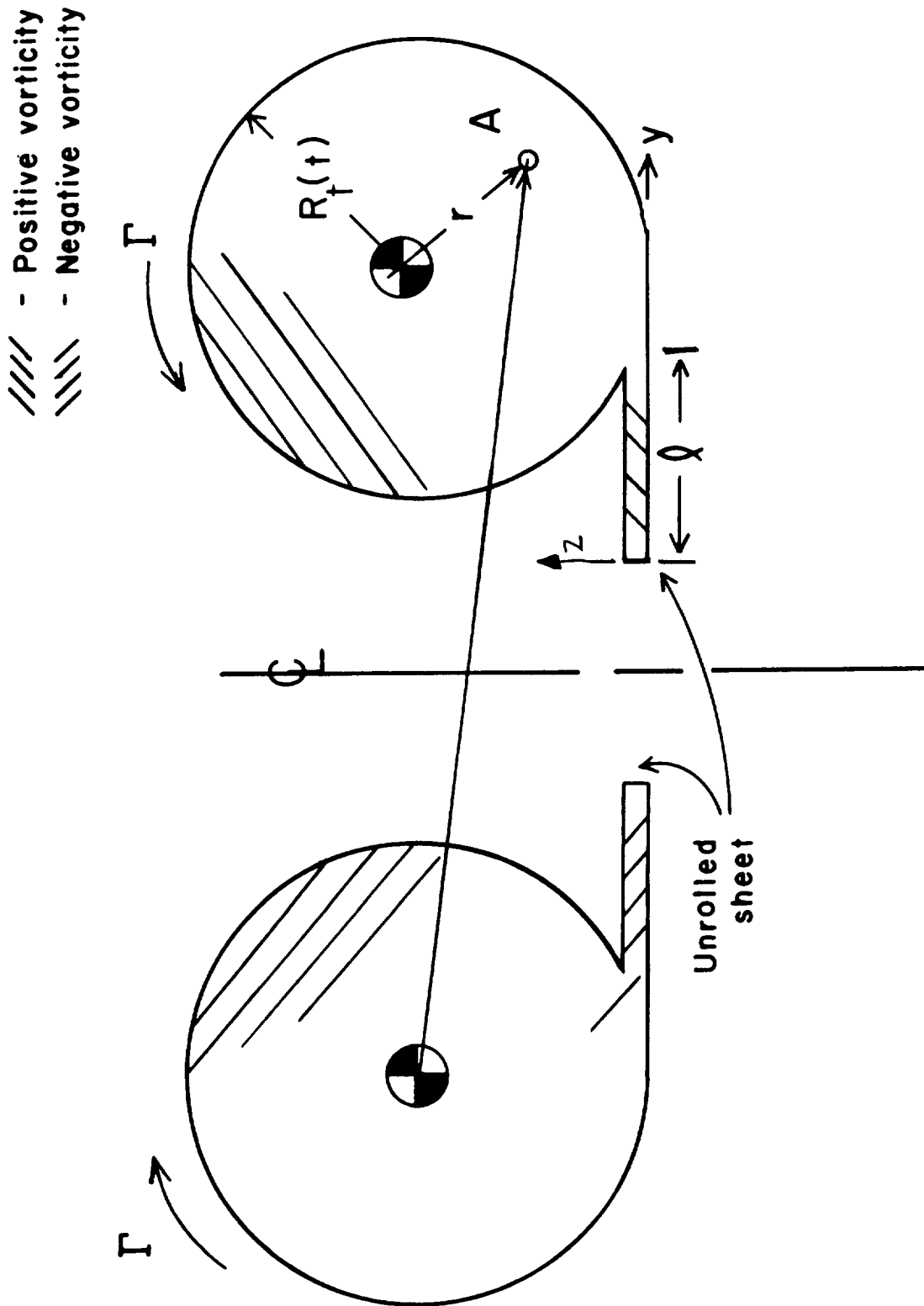


Figure 8. Schematic of how the velocity field at a particle position  $A$  is computed

where:

$$\begin{aligned} r_+^2 &= y^2 + z^2 \\ r_-^2 &= (y - \ell)^2 + z^2 \end{aligned} \tag{42}$$

and  $x$  is measured downstream of the wing and related to time by  $x = U_\infty t$ . A similar expression gives the velocity contribution from the unrolled up left sheet and its image sheets. The average circulation is given by:

$$\Gamma_{ave} = \frac{1}{\ell} \int_0^{\ell} \Gamma dy \tag{43}$$

where  $\ell$  is the unrolled length. On the sheet the velocity is singular, since the sheet is infinitely thin. In reality the velocity varies linearly across the sheet. In the AGDISP code this linear variation is assumed to occur over a length equal to  $0.1\ell$ .

The contributions of the rolled up portion of the vortices are similar. The velocity is of magnitude:

$$|U| = \frac{\Gamma(r)}{2\pi r} \tag{44}$$

where  $r$  is the distance from the centroid of the vortex to the particle position. The left and right vortices and their image vortices contribute to the magnitude of the velocity at the particle position by summing the contributions from Eq. (44). The velocity contribution of each vortex is perpendicular to a line connecting the vortex centroid and the particle position.

In summary, the fixed wing wake flow field model is quite detailed and accounts for wake roll up and descent as well as for velocity field variations resulting from the details of the spanwise load distribution. The user may also elect to forgo this detail by specifying the position and strength of fully rolled up point vortices.

### Helicopter Flow Field

The wake of a helicopter is considerably more complex than the wake of a fixed wing aircraft since the rotor downwash wake in hover is fluid dynamically different than the vortex wake generated by a fixed wing



aircraft. The flow field model included in the AGDISP code transitions from a hover wake at advance ratio  $\mu$  equal to zero, to a vortex wake at advance ratio equal to  $\mu_0$ . Figure 9 schematically shows the helicopter wake model option in the AGDISP code. The weight of the aircraft  $W$  is divided into a uniform downwash and a vortex wake according to:

$$\left(1 - \frac{\mu}{\mu_0}\right)W = 2\rho_{\text{air}}\pi R_r^2 U_3(h)^2 \quad (45)$$

$$\frac{\mu W}{\mu_0} = 2\rho_{\text{air}} U_\infty \Gamma_r R_r \quad (46)$$

where  $U_3(h)$  is the induced velocity at the rotor computed from actuator disk theory and  $R_r$  is the rotor radius. For values of  $\mu/\mu_0$  greater than unity, the complete weight of the helicopter is carried by the vortex wake. Eq. (46) defines the vortex strength  $\Gamma_r$  of the tip vortices positioned at the end of the blade. At zero advance ratio the wake induced velocity at the rotor plane is uniform across the actuator disk, while at an advance ratio of  $\mu_0$ , the entire wake resembles that of a fixed wing aircraft. Beneath the rotor the downwash velocity,  $U_3$ , from the actuator disk portion of the wake is assumed to decrease linearly to the surface as:

$$U_3(z) = U_3(h)z/h \quad (47)$$

where  $h$  is the rotor altitude above the ground.

Along the dividing streamline the pressure perturbation is zero, so that along this surface:

$$U_2^2 + U_3^2 = U_3(h)^2 \quad (48)$$

Since the flow is tangent to this surface:

$$\frac{dz_s}{dy_s} = \frac{U_3}{U_2} = -\frac{z_s}{h} \frac{1}{\sqrt{1 - \left(\frac{z_s}{h}\right)^2}} \quad (49)$$

where the subscript  $s$  denotes the location of the dividing streamline. Integrating Eq. (49), subject to  $z_s = h$ ,  $y_s = R_r$  yields:

$$\frac{y_s}{h} = \frac{R_r}{h} - \sqrt{1 - \left(\frac{z_s}{h}\right)^2} \ln \left[ \frac{1 + \sqrt{1 - \left(\frac{z_s}{h}\right)^2}}{\frac{z_s}{h}} \right] \quad (50)$$

for the  $y_s$  position of the dividing streamline given the  $z_s$  position of the dividing streamline. If a particle is located outboard of the dividing streamline, it will feel no effect of the helicopter downwash field. If a particle is within the downwash field, however, it will experience a downward velocity component given by Eq. (47) and a horizontal velocity component assumed to be linear from the wake centerline as:

$$U_2 = -U_3(h) \frac{y}{y_s} \sqrt{1 - \left(\frac{z_s}{h}\right)^2} \quad (51)$$

When the advance ratio is zero the flow field is described by Eq. (47), (49) and (51) and the flow is contained in the initial plane shown in Figure 9 ( $x = 0$  since  $U_\infty = 0$ ). For non-zero advance ratios the initial plane moves downstream at velocity  $U_\infty$  and the agricultural material see the cross flow field resulting from a wake skewed downstream by the free stream. In addition, at non-zero advance ratios, a vortex pair flow field is added to the cross flow plane. The vortex strength  $\Gamma_r$  is computed from Eq. (46) and the initial separation between vortices is the rotor diameter  $2R_r$ .

The position of the centerline of the skewed wake is given by integrating:

$$\frac{dz_{cr}}{dx} = \frac{U_3}{U_\infty} = \frac{U_3(h)}{U_\infty} \frac{z}{h} \quad (52)$$

with  $z = h$  at  $x = 0$ . The integration yields:

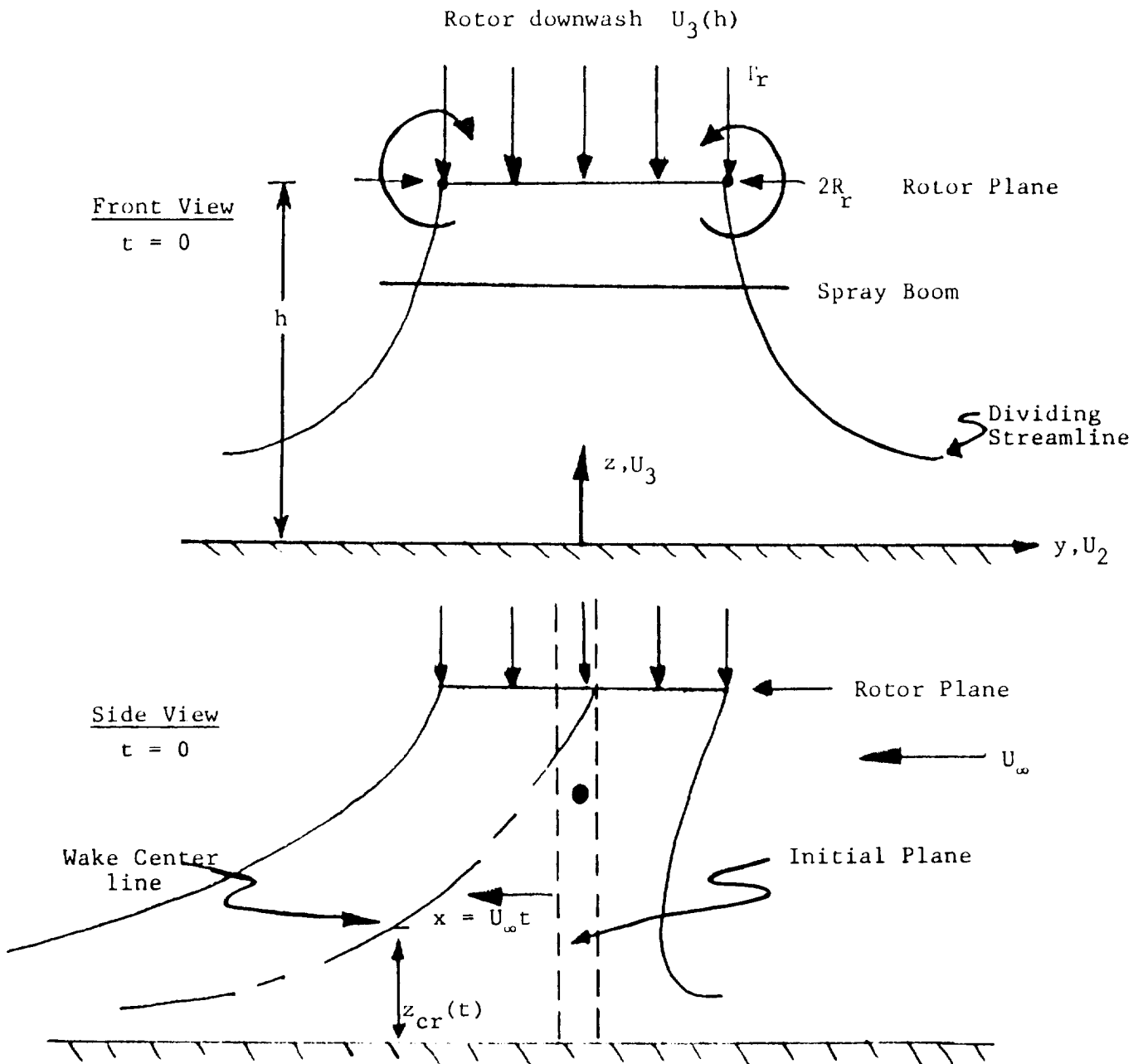


Figure 9. Schematic of the helicopter flow field model

$$\frac{z_{cr}}{h} = \exp\left(\frac{U_3(h)x}{U_\infty h}\right). \quad (53)$$

### Propeller Swirl

Fixed wing aircraft propulsion systems utilize a propeller driven by either a piston or turbo jet engine. The propeller flow field modeling in the AGDISP code treats the propeller as an actuator disk. At the disk the incremental velocity  $\Delta U_1$  over the flight speed  $U_\infty$  is related to the thrust  $T$  by:

$$T = 2\rho_{air}\pi R_p^2 \Delta U_1 (U_\infty + \Delta U_1) \quad (54)$$

where  $R_p$  is the propeller radius. In steady flight the thrust equals the drag so that:

$$T = D = C_D \frac{1}{2} \rho_{air} U_\infty^2 S \quad (55)$$

where  $S$  is the wing planform area and  $C_D$  is the aircraft drag coefficient. Combining Eqs. (54) and (55) to eliminate  $T$ , we obtain the induced velocity at the disk:

$$\frac{\Delta U_1}{U_\infty} = - \frac{1 + \sqrt{1 + \frac{C_D S}{A}}}{2} \quad (56)$$

The propeller exerts a torque  $Q$  on the fluid resulting in an axial flux of angular momentum downstream of the actuator disk. If we assume that the distribution of swirling velocity is linear in distance from the propeller axis, then the axial flux of angular momentum may be computed as:

$$Q = 2\pi \int_0^R \rho_{air} r^2 \Omega_p (U_\infty + \Delta U_1) r dr = \frac{\pi}{2} \rho_{air} \Omega_p^2 R_p^4 (U_\infty + \Delta U_1) \quad (57)$$

where  $\Omega_p$  is the angular velocity of the propeller. The useful power produced by a propeller is the thrust times the flight speed. This power is related to the actual power supplied to the hub through a propeller efficiency coefficient  $\eta$  :

$$TU_\infty = \eta Q \Omega_q \quad (58)$$

where  $\Omega_q$  is the propeller rotational speed. Combining Eqs. (57) and (58) together with Eq. (55) yields:

$$\Omega_p = \frac{U_\infty^3 C_D S}{\pi \eta \Omega_q R_p^4 (U_\infty + \Delta U_1)} \quad (59)$$

showing that the swirl left in the propeller slip stream increases with decreasing propeller efficiency.

Downstream of the actuator disk the propeller slip stream spreads primarily as a consequence of turbulent diffusion. At the actuator disk the mean squared turbulence level computed from superequilibrium theory is:

$$q_p^2 = 2\Lambda^2 \left( \frac{\Delta U_1}{R_p} \right)^2 \quad (60)$$

where  $\Lambda$  is the turbulent integral scale and the gradient of slip stream velocity is estimated to be of the order of  $\Delta U_1/R_p$ . If the largest eddies are assumed to be 60% of the radius of the slip stream (an assumption often used in jet flow calculations), the turbulence level at the actuator disk becomes:

$$q_p^2 = 0.72 \Delta U_1^2 \quad (61)$$

By balancing the flux of turbulent kinetic energy in the slip stream with turbulent dissipation and assuming that the integral scale grows linearly with

downstream distance, the propeller wake area will grow as the square of the downstream distance. The turbulent kinetic energy downstream of the propeller in the slipstream can be shown to equal:

$$\frac{q^2}{q_p^2} = 0.86 \frac{U_\infty}{q_p} \left( \frac{x_0}{R_p} \right)^{0.18} \left( \frac{x + x_0}{R_p} \right)^{1.18} \quad (62)$$

where  $x_0$  is the virtual origin computed from Ref. 20 as:

$$x_0 = 1.4 U_\infty \Lambda / q_p \quad (63)$$

### Simple Terrain

To investigate the influence of surface slope on deposition pattern, a simple terrain model is included in the AGDISP code. The interaction of the vortex wake with an inclined straight ground plane (Figure 10) is incorporated by modifying the position of the image vortex system to retain the requirement of zero fluid velocity perpendicular to the inclined plane. The helicopter and Betz roll up effects are similarly modified.

### Cross-wind

Cross-wind flow can significantly alter the ground deposition pattern even when the aircraft is flying close to the surface. In a neutral atmospheric surface layer the horizontal velocity follows a logarithmic profile:

$$U_2(z) = U_2(z_d) \frac{\ln\left(\frac{z}{z_0}\right)}{\ln(z_d/z_0)} \quad (64)$$

where  $U_2(z_d)$  is the horizontal velocity perpendicular to the flight path at a given altitude  $z_d$ , and  $z_0$  is the surface roughness. This roughness is usually taken to be 1/30 of the actual physical roughness height.

Associated with this cross-wind profile is fluid turbulence resulting from the mean shear. With the assumption that the integral scale of turbulence is proportional to the distance from the surface ( $\Lambda = 0.65z$ ), the turbulent kinetic energy  $q^2$  becomes:

ORIGINAL PAGE IS  
OF POOR QUALITY

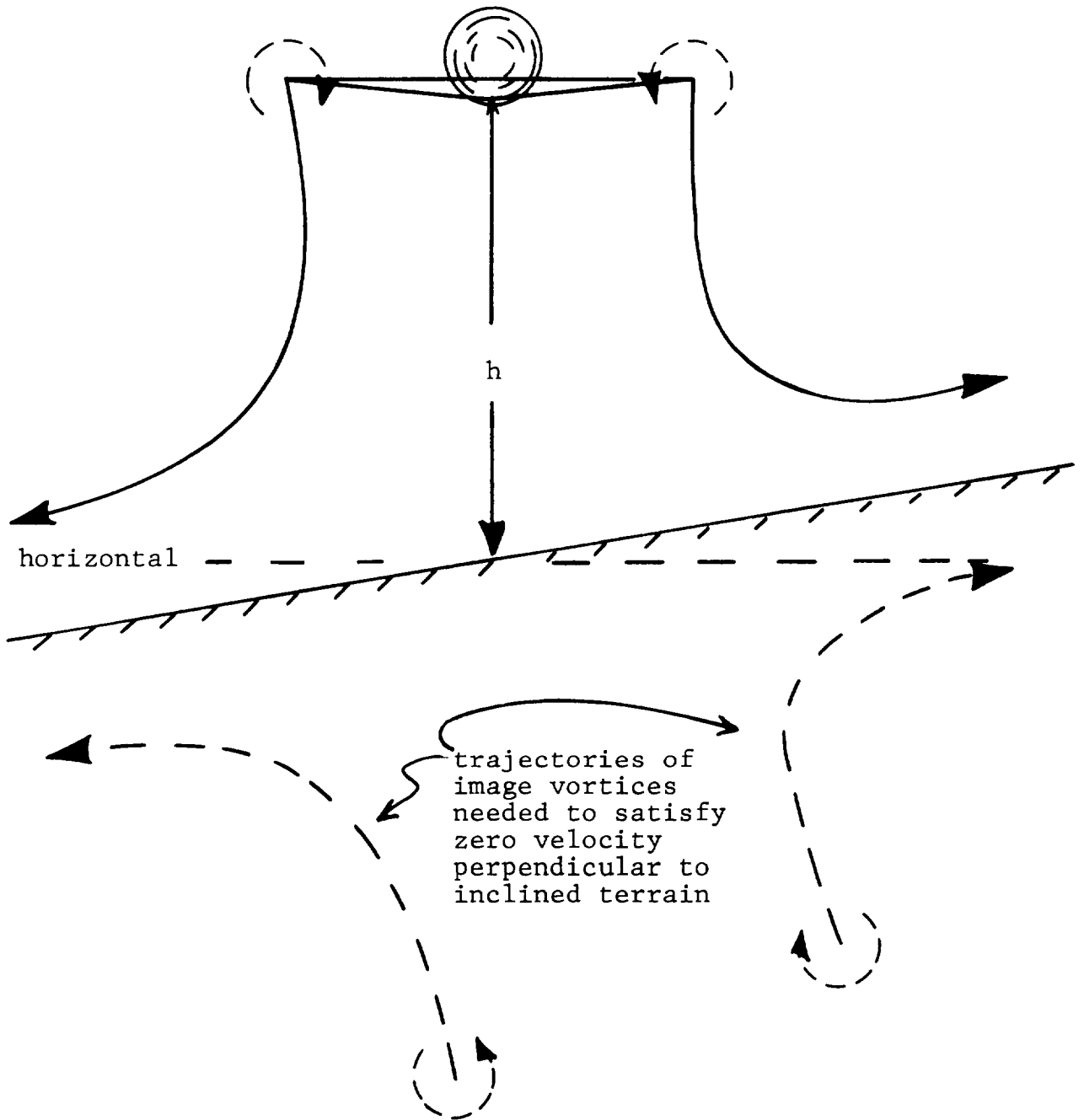


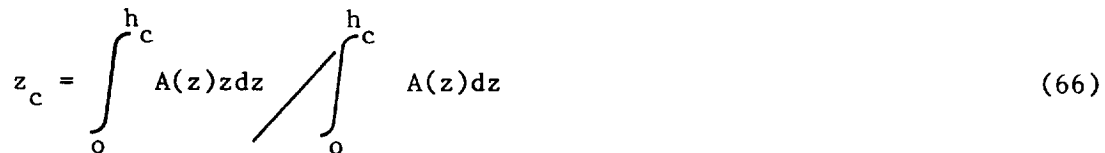
Figure 10. Vortex trajectories in the vicinity of inclined terrain

$$q^2 = \langle u_1 u_1 \rangle + \langle u_2 u_2 \rangle + \langle u_3 u_3 \rangle = \frac{0.845 U_2(z_d)^2}{[\ln(z_d/z_o)]^2} \quad (65)$$

The mean velocity logarithmic profile and its associated constant turbulence level are included in the AGDISP code.

### Plant Canopy

The canopy flow field model programmed in the AGDISP code is an approximation of the second-order closure turbulence model of Wilson and Shaw<sup>(21)</sup>. Figure 11 illustrates the canopy configuration. The canopy is assumed to be of height  $h_c$ , with a plant areal density denoted by  $A(z)$ . An effective canopy roughness height is defined as:

$$z_c = \int_0^{h_c} A(z)z dz \quad \int_0^{h_c} A(z) dz \quad (66)$$


so that the mean cross-wind velocity above the canopy may again be logarithmic and given by:

$$U_2(z) = U_2(z_d) \ln(z/z_c) / \ln(z_d/z_c) \quad , \quad z > h_c \quad (67)$$

The mean turbulence above the canopy is given by Eq. (65). The height  $z_c$  may be interpreted as the displacement thickness caused by the presence of the canopy.

Within the canopy itself the mean velocity and root mean square turbulence level are assumed to go to zero linearly as the ground ( $z=0$ ) is approached. This approximation is consistent with the Wilson and Shaw data as seen in Figure 11. Thus for  $z < h_c$ :

$$U_2(z) = \frac{z}{h_c} U_2(z_d) \ln(h_c/z_c) / \ln(z_d/z_c) \quad (68)$$



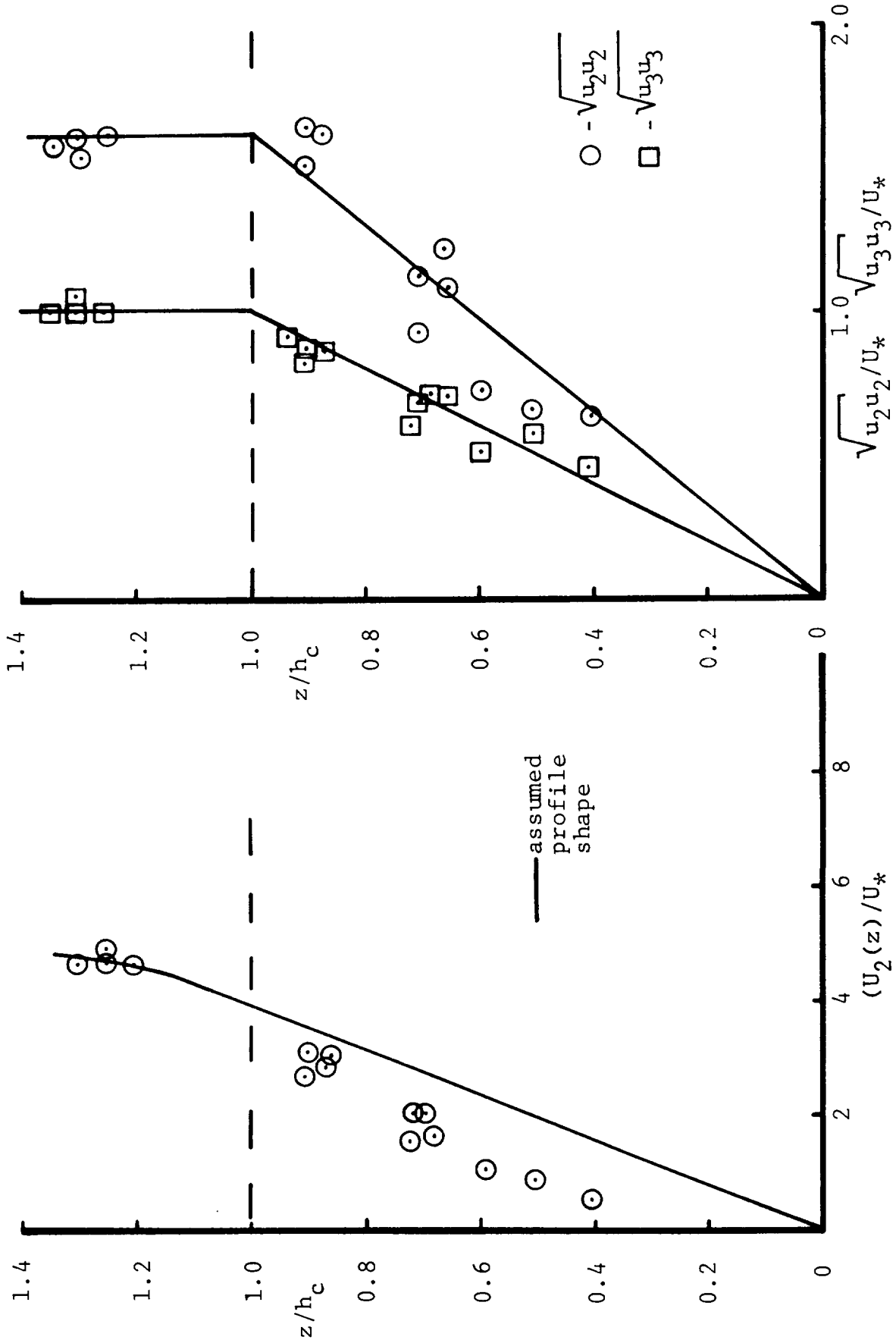


Figure 11. Mean wind and root mean square turbulent fluctuations in a canopy (Wilson & Shaw (21)).

Here  $U_* = U_2(z_d)/\ln(z_d/z_0)$

$$q^2 = 0.845 \left( \frac{z}{h_c} \right)^2 \frac{U_2(z_d)^2}{[\ln(z_d/z_c)]^2} \quad (69)$$

The canopy not only modifies the turbulence and wind shear above and within the canopy but also results in a drag force on the fluid in the wake descending into the canopy. In the AGDISP code this drag force acts on any vortex entering the canopy (for simplicity, the helicopter wake resulting from the nonvortex portion of the downwash flow field is assumed to not interact with the canopy). Figure 12 illustrates the entrance of a vortex into the canopy. The retarding effect of the canopy is estimated by assuming that the swirling velocity in the entering vortex is reduced by a square drag law when entering the canopy:

$$\frac{d\sqrt{U_2^2 + U_3^2}}{dt} (r,t) = - C_C A(z) (U_2^2 + U_3^2) \quad (70)$$

Since it is the circulation reduction that slows down the vortex in the canopy, Eq. (70) is recast by substituting  $\Gamma = \pi \bar{b} \sqrt{U_2^2 + U_3^2}$  and defining a depth-averaged plant areal density as:

$$\bar{A} = \frac{1}{a} \int_{h-a}^h A dz \quad (71)$$

where  $a$  is the penetration depth of the vortex (as shown in Figure 12). If we assume that the retarding effect of the canopy will be proportional to that portion of the vortex flow field immersed in the canopy, Eq. (70) can be recast to become:

$$\frac{d\Gamma}{\Gamma^2} = - \frac{C_C \bar{A} A' dt}{\pi \bar{b} A_T} \quad (72)$$

where  $A'/A_T$  is the fraction of the vortex within the canopy. At  $t = 0$  we set  $\Gamma = \Gamma_0$  so that Eq. (72) yields:

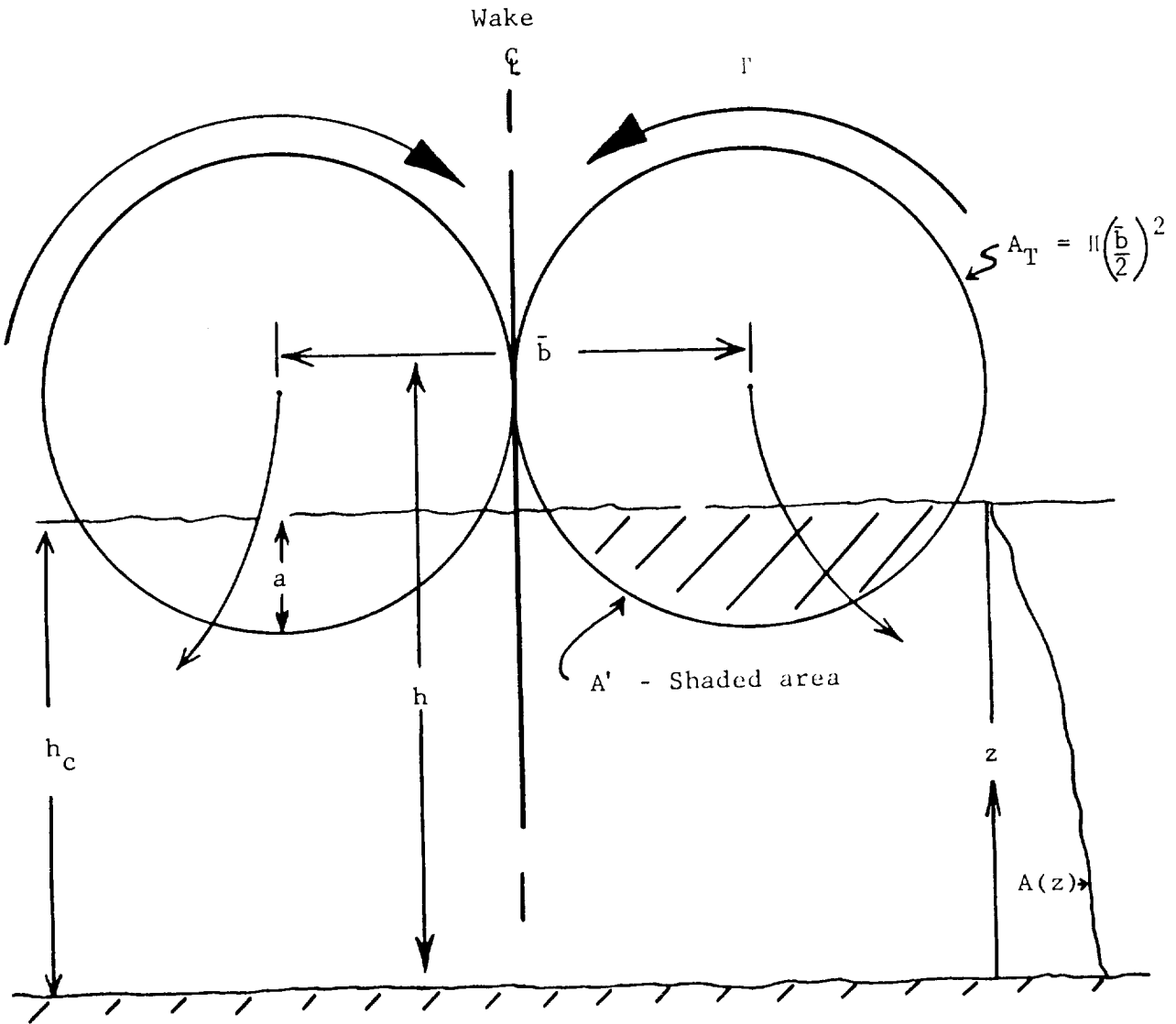


Figure 12. Schematic of a vortex wake entering into a plant canopy

$$\frac{\Gamma}{\Gamma_0} = \frac{1}{1 + \frac{0}{\pi \bar{b}} F(t)} \quad (73)$$

where

$$F(t) = \int_0^t C_C \bar{A} \frac{A'}{A_T} dt \quad (74)$$

Since  $F(t)$  is a monotonically increasing function of time, the effect of the canopy is to continually reduce the circulation of the vortex as it interacts with the canopy. The result of this reduction in circulation is a decrease in the descent rate of the vortex pair as it moves into the canopy, as well as a reduction in the swirling velocities and the wake convection of agricultural material. Consequently, a particle entering the canopy in the presence of cross-wind will feel a gradually reduced local velocity field tending to decelerate the particle. Vortices entering the canopy will become less effective in influencing particle motion because of the reduction in their circulation strength as given by Eq. (73).

### Superequilibrium Turbulence

The option of including the detailed effects of turbulence on the dispersion of agricultural material is incorporated in the AGDISP code by invoking superequilibrium turbulent transport theory<sup>(22)</sup>. Superequilibrium refers to the second-order closure turbulent transport model limit where the velocity correlations are able to track their equilibrium values. This limit is also referred to as the eddy viscosity limit, since velocity correlations are proportional to mean velocity gradients. For an incompressible flow the diffusion-free second-order correlations  $\langle u_i u_j \rangle$  satisfy:

$$\begin{aligned} \frac{D\langle u_i u_j \rangle}{Dt} = & - \frac{\partial U_m}{\partial x_n} \underbrace{\left[ \delta_{im} \langle u_n u_j \rangle + \delta_{mj} \langle u_i u_n \rangle \right]}_{\text{Production}} \\ & + \frac{q}{\Lambda} \underbrace{\left[ \langle u_i u_j \rangle - \delta_{ij} \frac{q^2}{3} \right]}_{\text{Tendency to isotropy}} - \underbrace{\frac{\delta_{ij}}{12} \frac{q^3}{\Lambda}}_{\text{Dissipation}} \end{aligned} \quad (75)$$

where  $q^2 = \langle u_1 u_1 \rangle + \langle u_2 u_2 \rangle + \langle u_3 u_3 \rangle$  and repeated indices are summed. If the velocity correlations track the mean flow,  $D\langle u_i u_j \rangle / Dt = 0$ , and:

$$\frac{\partial U_m}{\partial x_n} \left[ \delta_{im} \langle u_n u_j \rangle + \delta_{mj} \langle u_i u_n \rangle \right] + \frac{q}{\Lambda} \left[ \langle u_i u_j \rangle - \frac{1}{3} \delta_{ij} q^2 \right] - \frac{\delta_{ij}}{12} \frac{q^3}{\Lambda} = 0 \quad (76)$$

Since the local mean flow gradients are known, the system of equations represented by Eq. (76) can be solved exactly for  $\langle u_i u_j \rangle$  to determine  $q^2$  for the evaluation of particle dispersion.

#### 4. APPLICABILITY OF AGDISP FOR LONG TIME DEPOSITION STUDIES

The AGDISP code computes the motion of clusters of particles released from a single nozzle by predicting the ensemble averaged mean trajectory and variance about this mean. Since the flow field through which these particles pass is in general inhomogeneous, that is, the ensemble averaged mean velocity field,  $U_i$ , and hence the mean square turbulence field,  $q^2$ , are in general functions of position, there are restrictions with regard to spatial scales over which code predictions are accurate.

A spatial scale defined by:

$$L_{TS} = q^2 \left/ \left| \frac{dq^2}{dz} \right| \right. \quad (77)$$

may be seen to be a characteristic length over which the turbulent flow field changes significantly. Since the dispersion of the released material is predicted by assuming that fluid fluctuations acting on the cluster of particles are those fluctuations existing at the mean position, a simulation time may eventually be reached where variance of the cluster of particles will be on the order of  $L_{TS}$ . At this point an error is introduced in the AGDISP prediction of variance.

Code predictions of dispersion are then reliable when the particle variance  $\langle x_i x_i \rangle$  is such that:

$$\langle x_i x_i \rangle < L_{TS}^2 \quad (78)$$

Code predictions of variance may still be useful past this point, but the user should be aware of the approximation being made to estimate the variance.

## 5. AGDISP VALIDATION AND SAMPLE CASES

Validation of the AGDISP code was undertaken by NASA and is documented in Ref. 23. Validation was made by comparing predicted deposition patterns against full scale measurements of deposition behind a fixed wing aircraft. To date, the code has not been validated for aerial application behind helicopters.

A limited number of sample calculations are presented here to illustrate some of the deposition problems which may be investigated with the code. Note that in all calculations presented here the particle density is taken to be that of water.

### Helicopter with Boom Extending Outboard of a Rotor

It is known that mounting a spray boom significantly outboard of the rotor may not necessarily increase swath width. A sample calculation is undertaken for a hypothetical helicopter with a gross weight of 13800 N and a rotor diameter of 8m. The spray boom is 6m above the ground, and the helicopter advance ratio is 0.2. The particles released from the boom have a specific gravity of unity and are 100  $\mu\text{m}$  diameter.

Results of the computation are presented in Figure 13 where trajectories are shown for times up to 50 seconds after helicopter passage. It is clear that material released outboard of the rotor do not feel the favorable downwash of the rotor and remain adrift. The outward and initially upward motion of these outboard particles result from the portion of the helicopter wake which is vortex like since the advance ratio is non-zero. It is clear that the AGDISP code can be utilized to investigate optimal boom location and positioning of nozzles for a specific spray mission.

### Material Release in a Neutral Turbulent Atmospheric Boundary Layer

In the AGDISP code the neutral atmospheric boundary layer has an assumed mean velocity profile which is logarithmic with altitude, while the atmospheric turbulence intensity is independent of altitude. Two computations are undertaken to illustrate the cross-wind effect. In the first (shown in Figure 14) particles of diameter 1000, 100 and 10  $\mu\text{m}$  with specific gravity equal to unity are released from rest at an altitude of 6.2m. The mean wind at 6m is taken to be 0.6 m/sec with the surface roughness of 0.03m. This results in an rms turbulent velocity fluctuation of 0.1 m/sec independent of height in the neutral layer. As may be seen, the mean trajectory and dispersion are a very strong function of particle diameter. The dashed lines about the solid mean is the standard deviation of the particle computed normal to the trajectory. In Figure 15 particles of 100  $\mu\text{m}$  diameter are released from rest at an altitude of 6.2m. The wind velocity at the release altitude is taken to be 0.6m and 1.5 m/sec. As anticipated the downstream point of impact and dispersion increase with higher wind speed. The greater dispersion results from the rms turbulent level increasing from 0.1 m/sec with a wind of 0.6 m/sec at 6m to 0.25 m/sec with a wind of 1.5 m/sec at 6m.

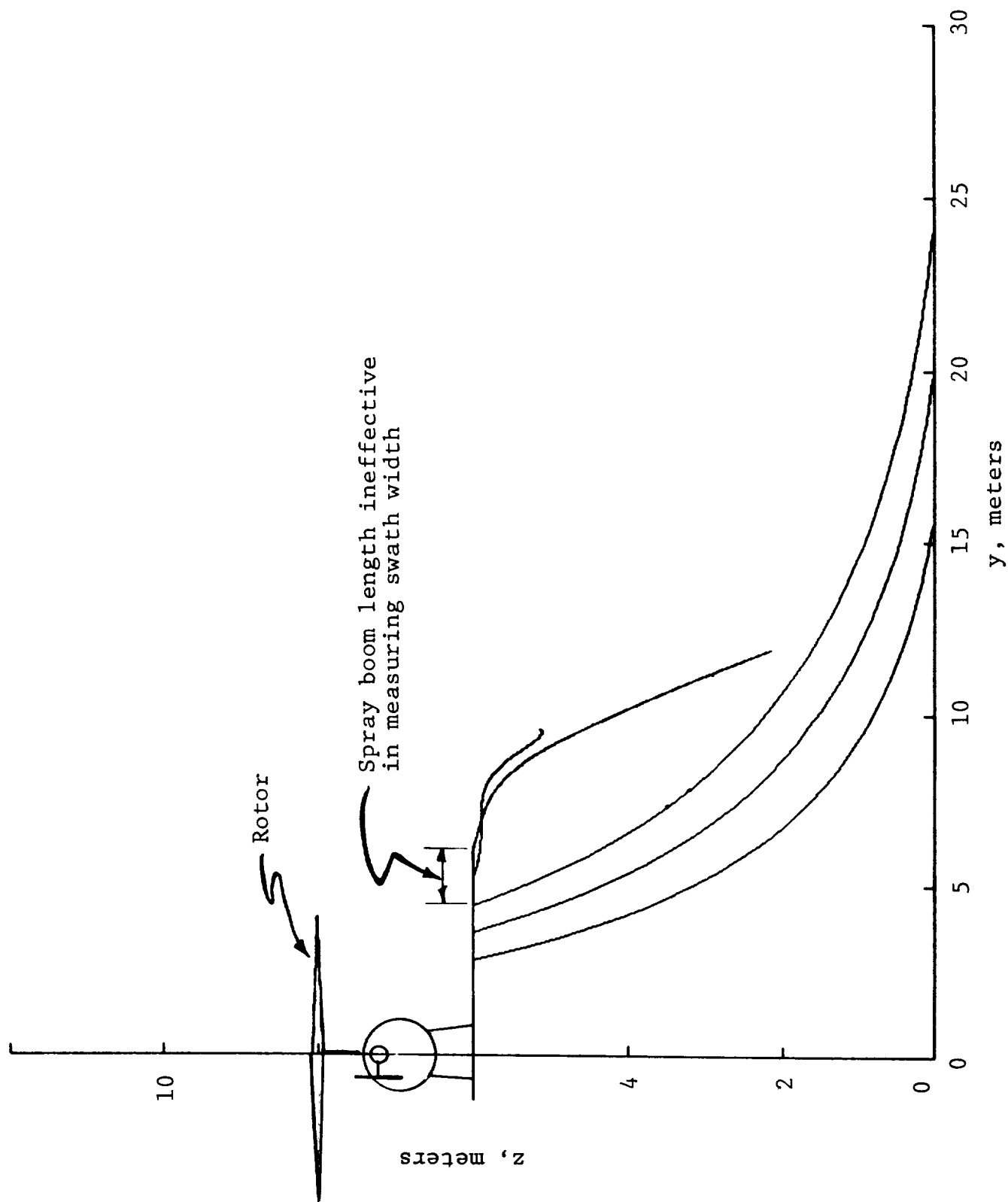


Figure 13. Aerial application from a helicopter with spray boom extended outboard of rotor



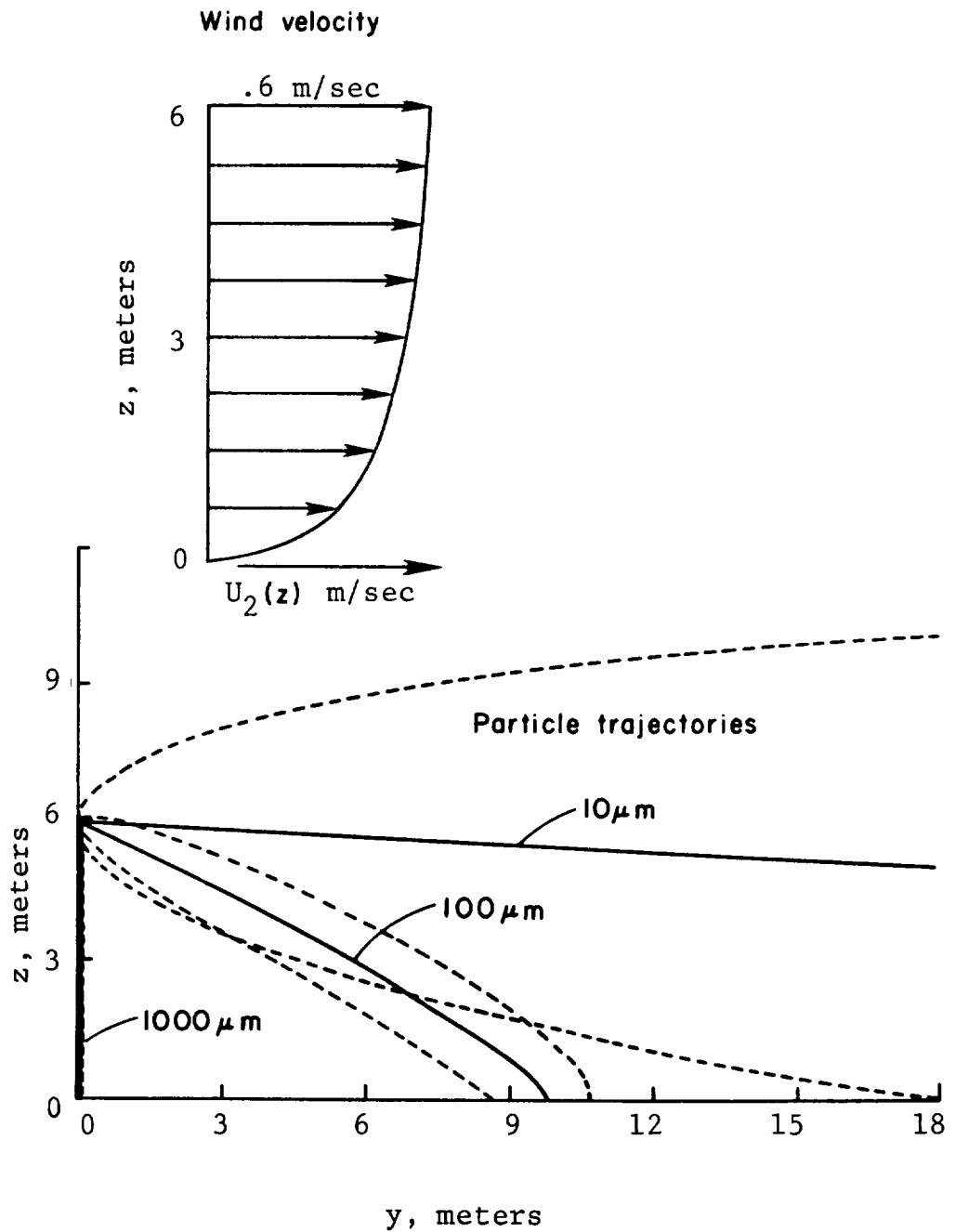


Figure 14. Mean particle trajectories (solid) and standard deviation in a direction perpendicular to the mean (dashed). Particles of diameter 10, 100 and 1000  $\mu\text{m}$  released from rest at an altitude of 6 m. Mean wind at 6 m was 0.6 m/sec.

ORIGINAL PAGE IF  
OF POOR QUALITY

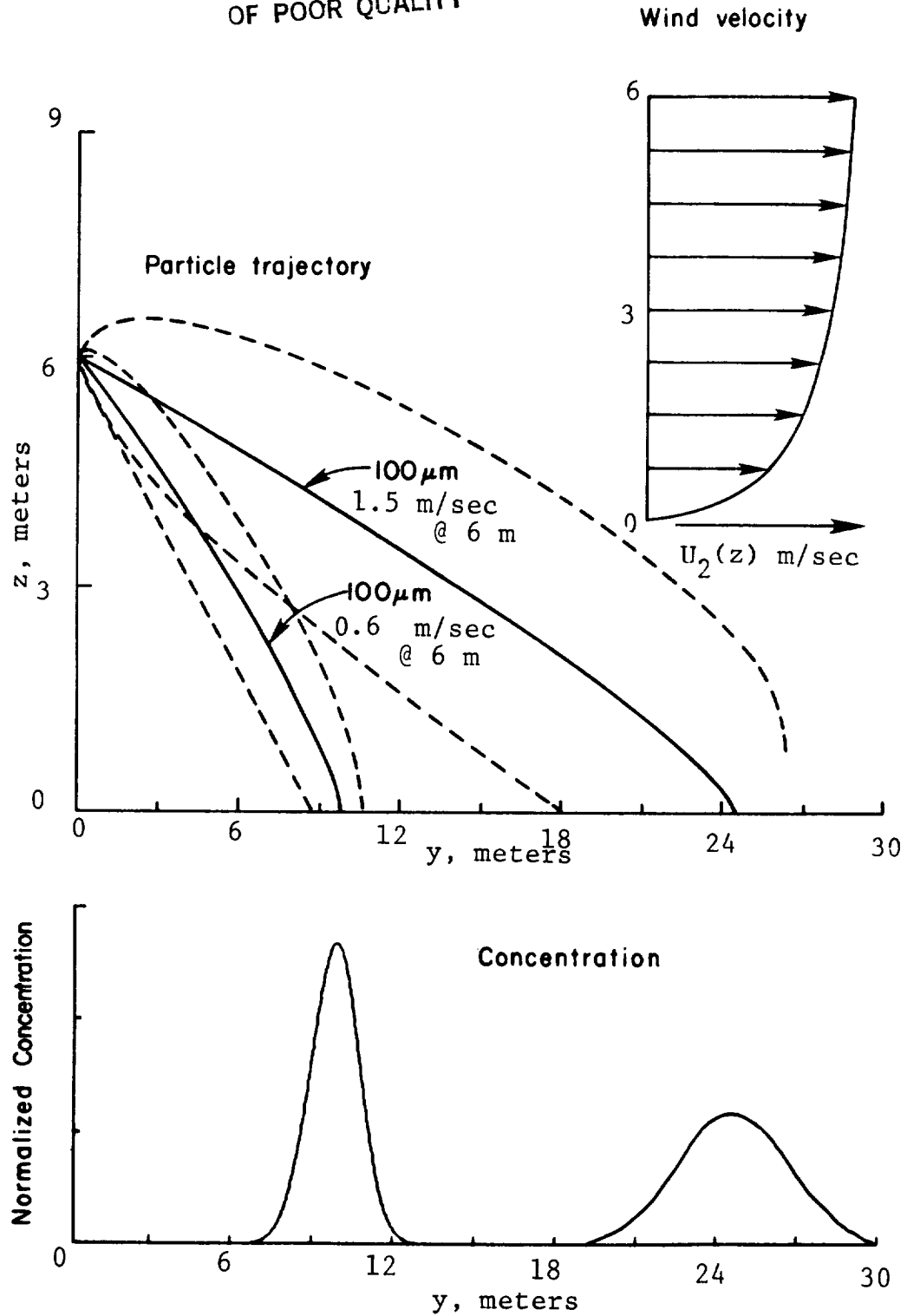


Figure 15. Effect of cross-wind magnitude on particle trajectory and on ground deposition pattern.  $100 \mu\text{m}$  particles are released from rest at an altitude of 6 m. Mean particle trajectory is shown solid and one standard deviation normal to the trajectory is shown dashed.

## Fixed Wing Aircraft with Triangular and Rectangular Spanwise Load Distribution

It is known that the spanwise load distribution of an aircraft can significantly alter the ground deposition pattern of material released into the wake. To illustrate this effect two load distributions are considered: a wing which is triangularly loaded and a wing which is rectangularly loaded. To put the predictions of ground deposition on a consistent basis, it is assumed that aircraft weight, wing span, flight speed and altitude are the same between wing loadings. In the calculations undertaken here, wake roll up is neglected and it is assumed that the trailing vortices at the wing are located at the centroid of vorticity and downstream descend under their mutual influence. Referring to Figure 16 it may be shown<sup>(17)</sup> that the swirling velocity of fully rolled up vortices from a triangularly loaded wing is

$$\begin{aligned} |U| &= \frac{2\Gamma_T}{\pi b} \quad , \quad r < b/4 \quad \text{and} \\ |U| &= \frac{\Gamma_T}{2\pi r} \quad , \quad r > b/4 \end{aligned} \tag{79}$$

and from a rectangularly loaded wing is:

$$|U| = \frac{\Gamma r}{2\pi r} \quad \text{for all } r \tag{80}$$

where  $r$  is measured from  $y = \bar{b}/2$  at the wing elevation. In these calculations the wing span is 6.2m and particles are released from wing elevation at lateral positions which are 0,  $\pm 17$ ,  $\pm 33$ ,  $\pm 50$ ,  $\pm 66$  and  $\pm 83$  percent of the semispan. It was assumed for convenience that the initial variance in particle position  $\langle x_i x_i \rangle$  and velocity  $\langle v_i v_i \rangle$  (no sum) were zero at the time of particle release. The required variances for fluid fluctuations were computed from the superequilibrium model described in Section 3.

Results of the simulation with AGDISP are shown in Figures 17 and 18. The mean trajectory is shown as a solid line, while the dotted curves denote the magnitude of the variance of particle position computed normal to the trajectory. The effect of load distribution on 100  $\mu\text{m}$  diameter particles is clearly seen. The higher wing root circulation in the triangularly loaded wing required to keep lift constant between computations results in particle trajectories being dominated by the vortices. In the rectangularly loaded case, only the particles released far outboard are dominated by the vortices. The results of these computations are, of course, not surprising since for a given particle size any reduction in the amount of swirling velocity in the wake is expected to diminish the influence of the wake on the deposition pattern.

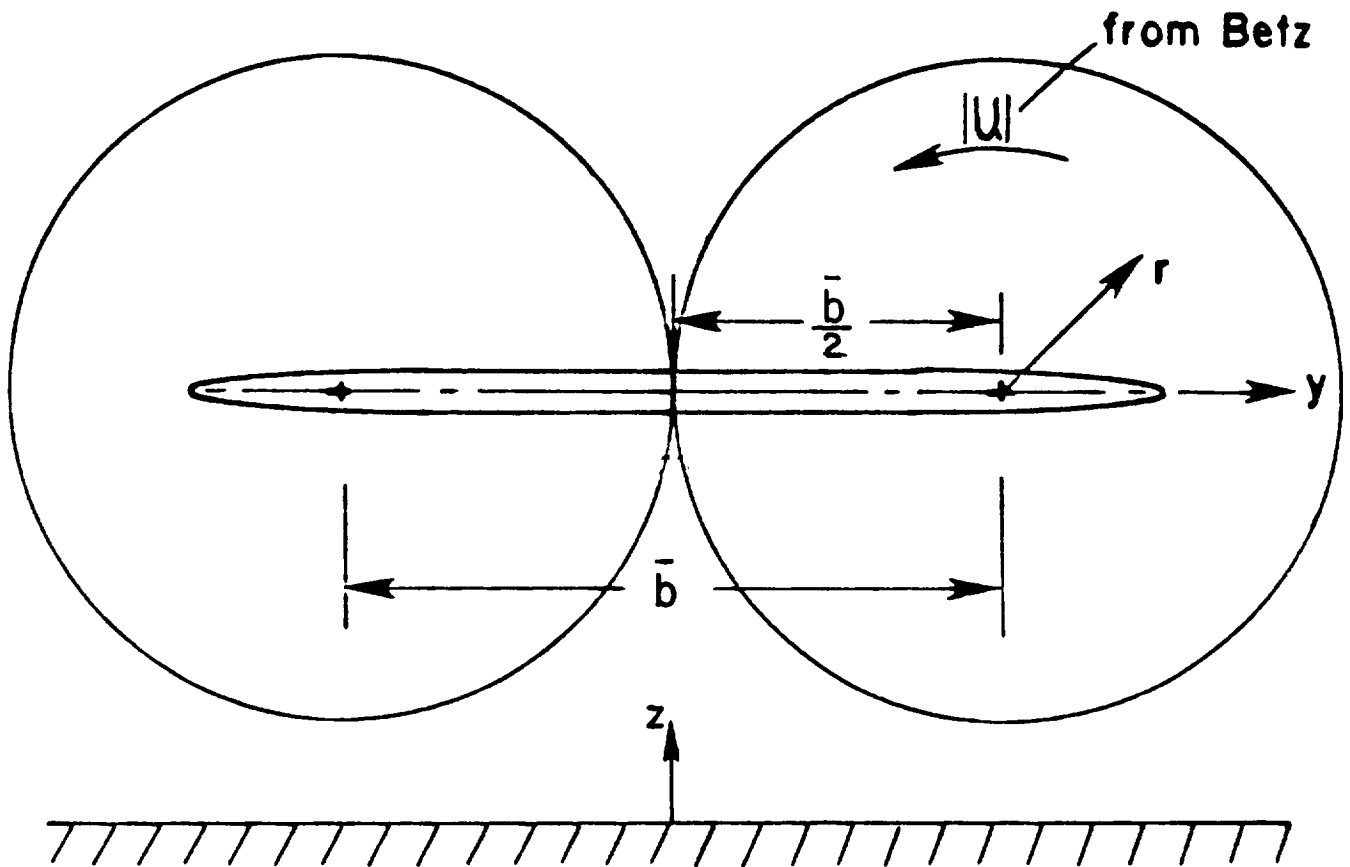


Figure 16. Geometric details of the wake flow field

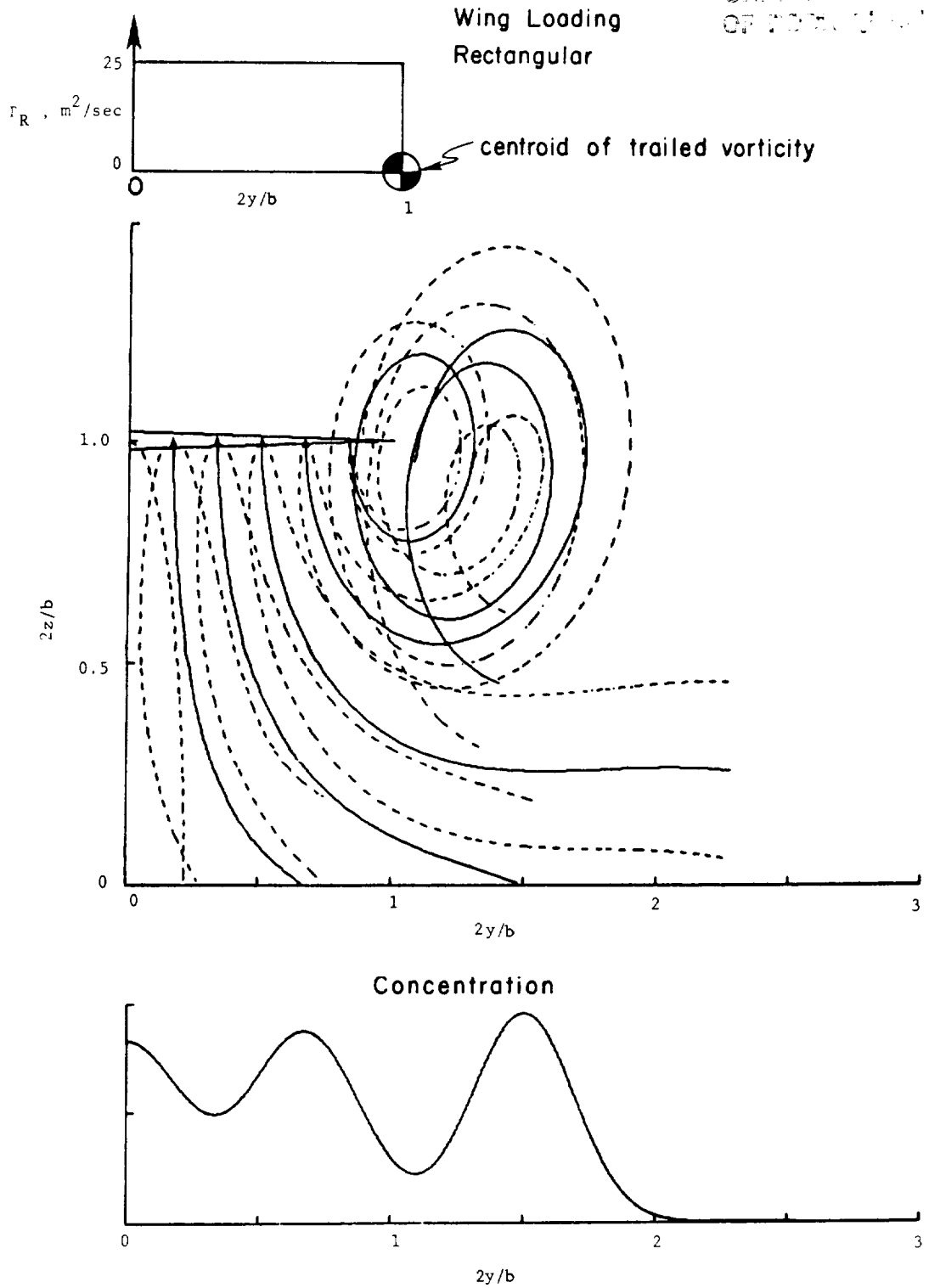


Figure 17. The particle trajectories and ground deposition pattern from a rectangularly loaded wing after 10 seconds of simulation. Mean trajectories are shown in solid and one standard deviation computed normal to the mean trajectory are shown dashed

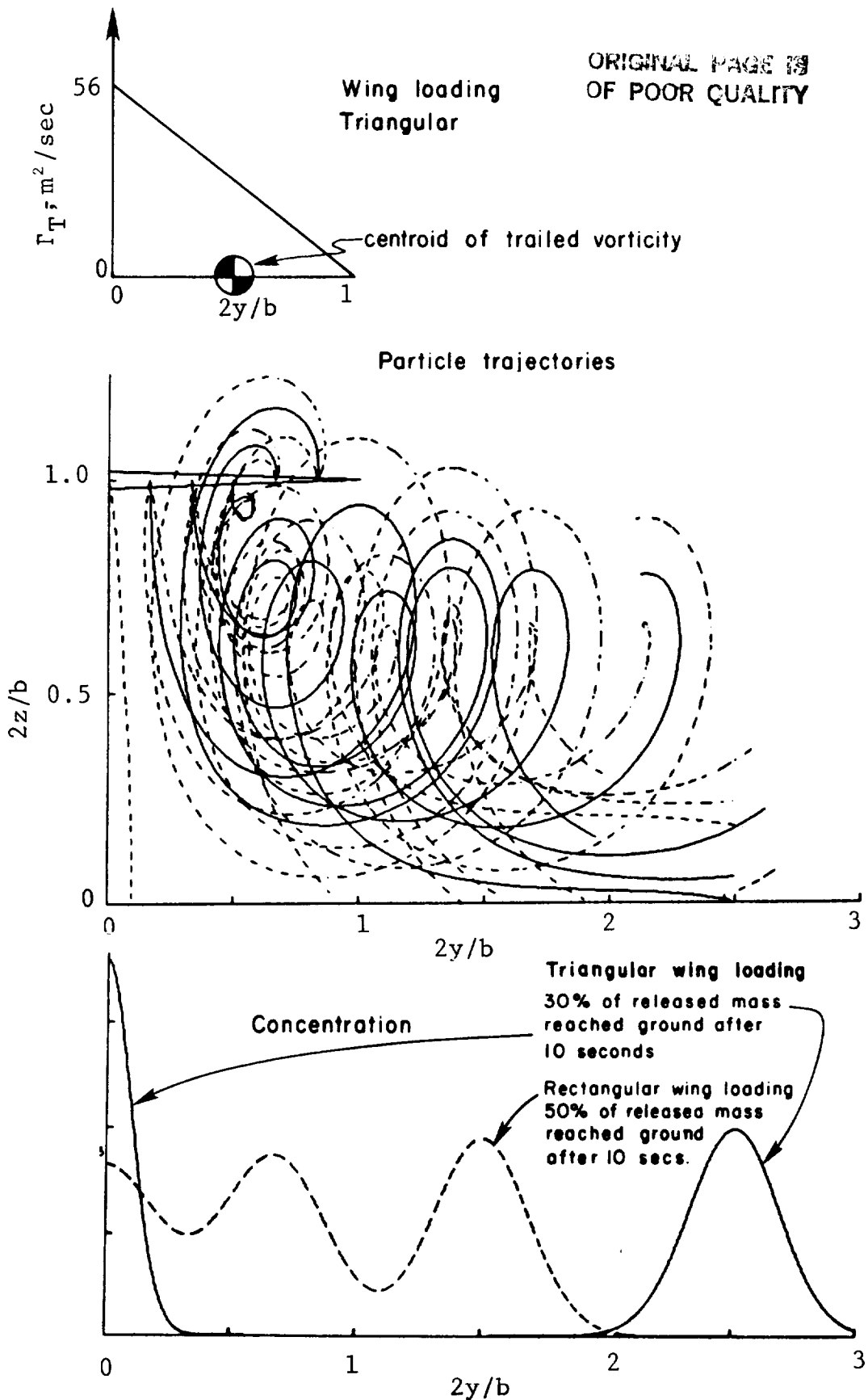


Figure 18. The particle trajectories and ground deposition pattern from a triangularly loaded wing after 10 seconds of simulation. A comparison of ground deposition pattern from a rectangularly loaded wing shown dashed is made with the deposition pattern from the triangularly loaded wing shown solid

### Cross-Wind

It is well known that the effect of cross-wind has a significant impact with regard to deposition pattern and resulting drift.

A calculation was undertaken with the horizontal velocity of 0.2 m/sec at 6m altitude, with the assumed logarithmic profile shape. The surface roughness was taken to be 3 cm and the rms turbulence level was 10.7 cm/sec. The particles were released at position  $\pm y = \pm 0.38n$  m with  $n$  taking integer values between 0 and 15. The results of this computation is shown in Figure 19 where the skewing of the deposition pattern on the ground is observed. The concentration distribution denoted by the dashed curve is the deposition pattern which results in the absence of cross-wind. It is noted that there results an excess in deposition upwind resulting from vortex swirling flow field countering the cross-wind.

### Evaporation

The effect of evaporation is to reduce particle diameter and hence make particle dynamics more sensitive to wake and atmospheric flow fields. A computation was made with the wet-bulb depression  $\Delta\theta = 5$  deg C identical to that illustrated in Figure 17 except that evaporation is permitted to occur. The results of the deposition computations are summarized in Figure 20 where it may be seen that when evaporation occurs there is nearly a factor of two reduction in mass deposited on the ground after 10 seconds.

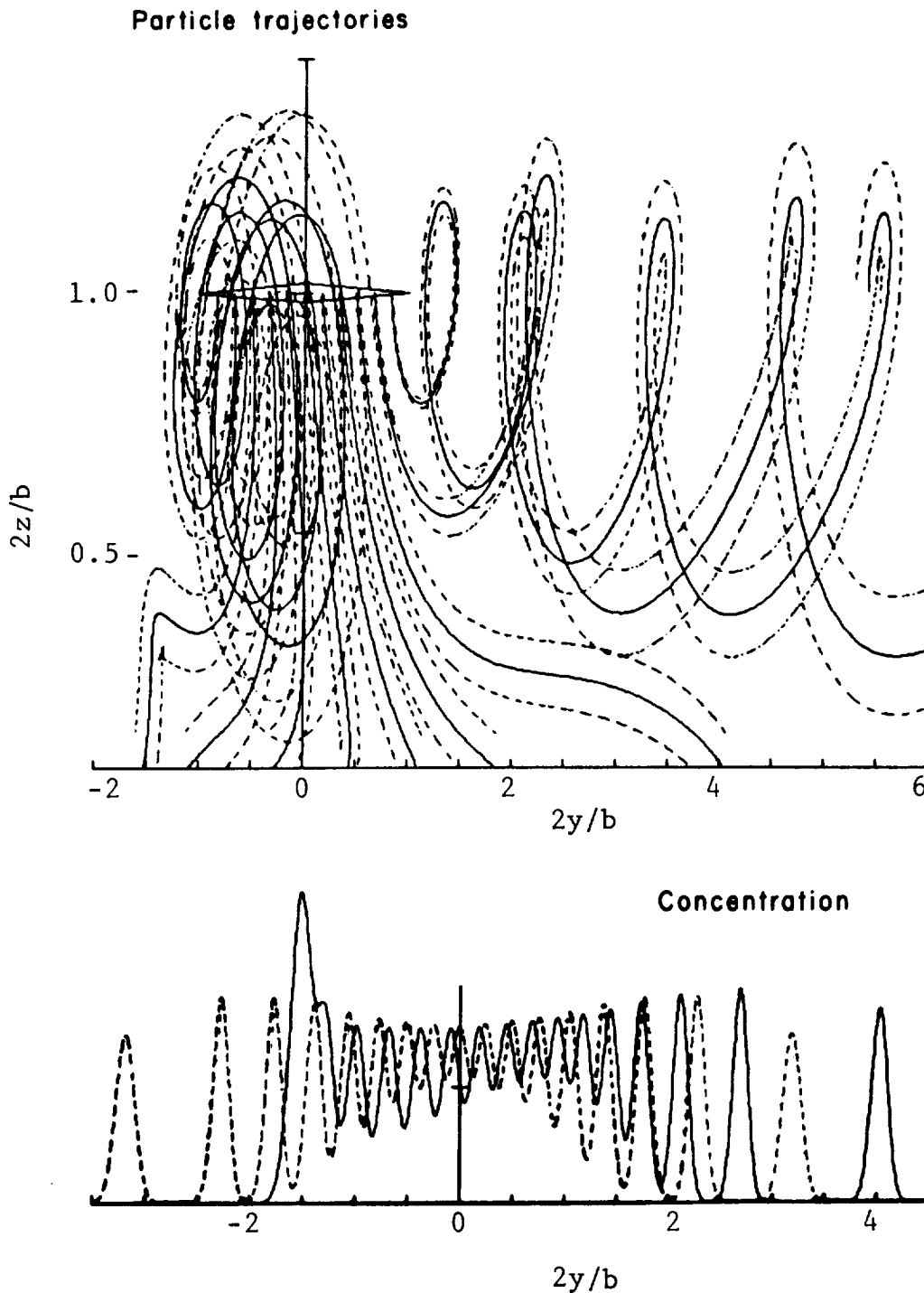


Figure 19. Effect of cross-wind on particle trajectories and ground deposition pattern. Solid and dashed curves on the concentration distribution are with and without a cross-wind respectively. The aircraft has a rectangular load distribution shown in Fig. 17.



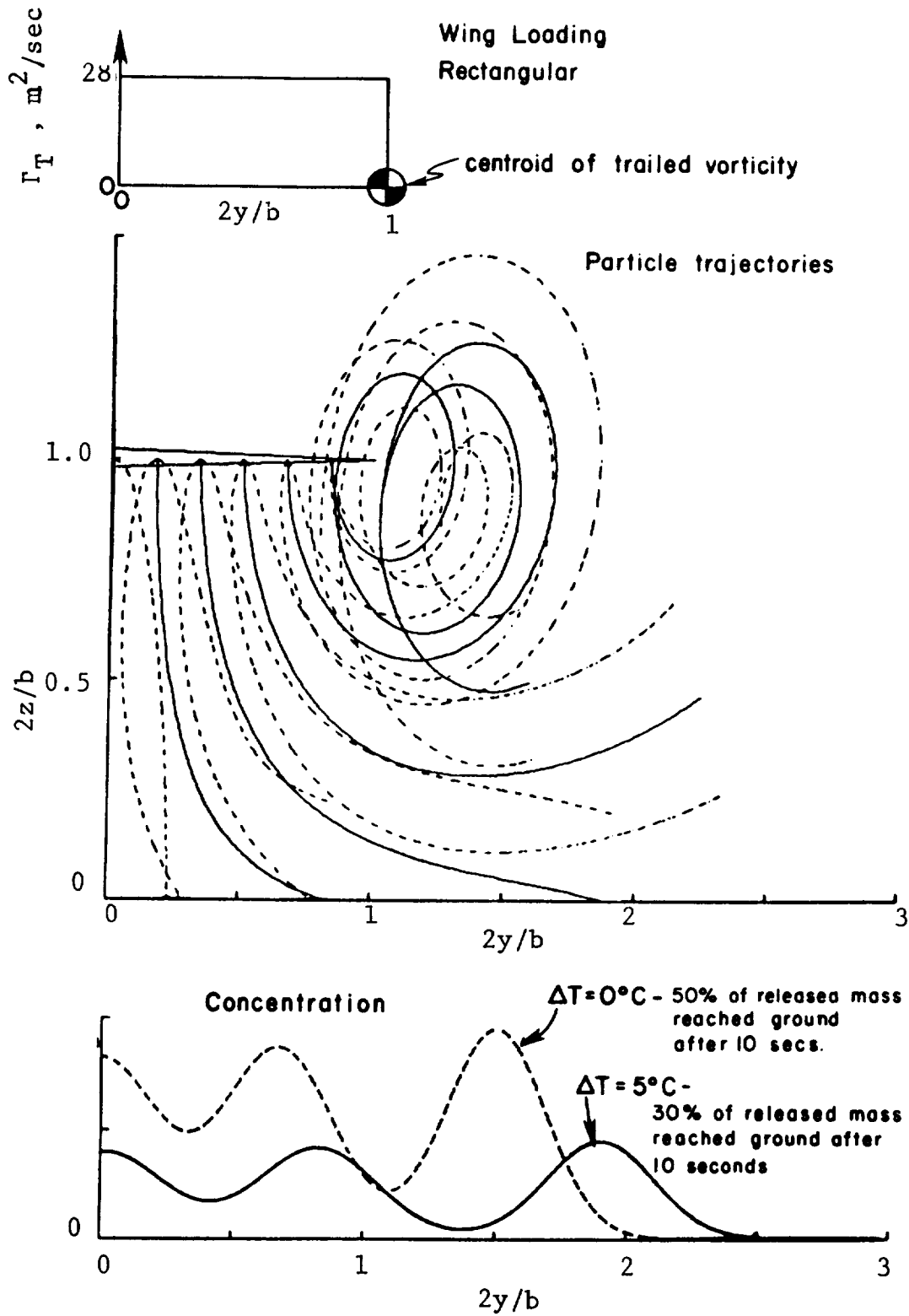


Figure 20. Effect of droplet evaporation on the ground deposition pattern

## 6. AGLINE

The AGDISP code tracks the dynamics of material released from discrete locations. After diffusion has had sufficient time to act, a spray cloud is formed and material can no longer be identified with the location from which it was released. To incorporate this smearing feature of turbulence diffusion, an option in the AGDISP code, "AGLINE" (AGricultural LINE Dispersal), can be exercised at any specified simulation time. This option replaces discrete distributions of material in the air with a single Gaussian distribution having the same mean and standard deviation as the discrete distributions. In this manner the AGDISP code can then be used to track the dynamics of a spray cloud or the AGLINE outputs can be used to initialize other dispersal codes.

Use of the AGLINE feature is documented in the AGDISP User Manual.<sup>(16)</sup> Figure 21 shows the results of using the AGLINE feature on the output of the sample calculation described in the User Manual. As can be seen in this example, four discrete distributions (dashed) are replaced by one distribution (solid) having the same mean and standard deviation.

ORIGINAL PAGE IS  
OF POOR QUALITY

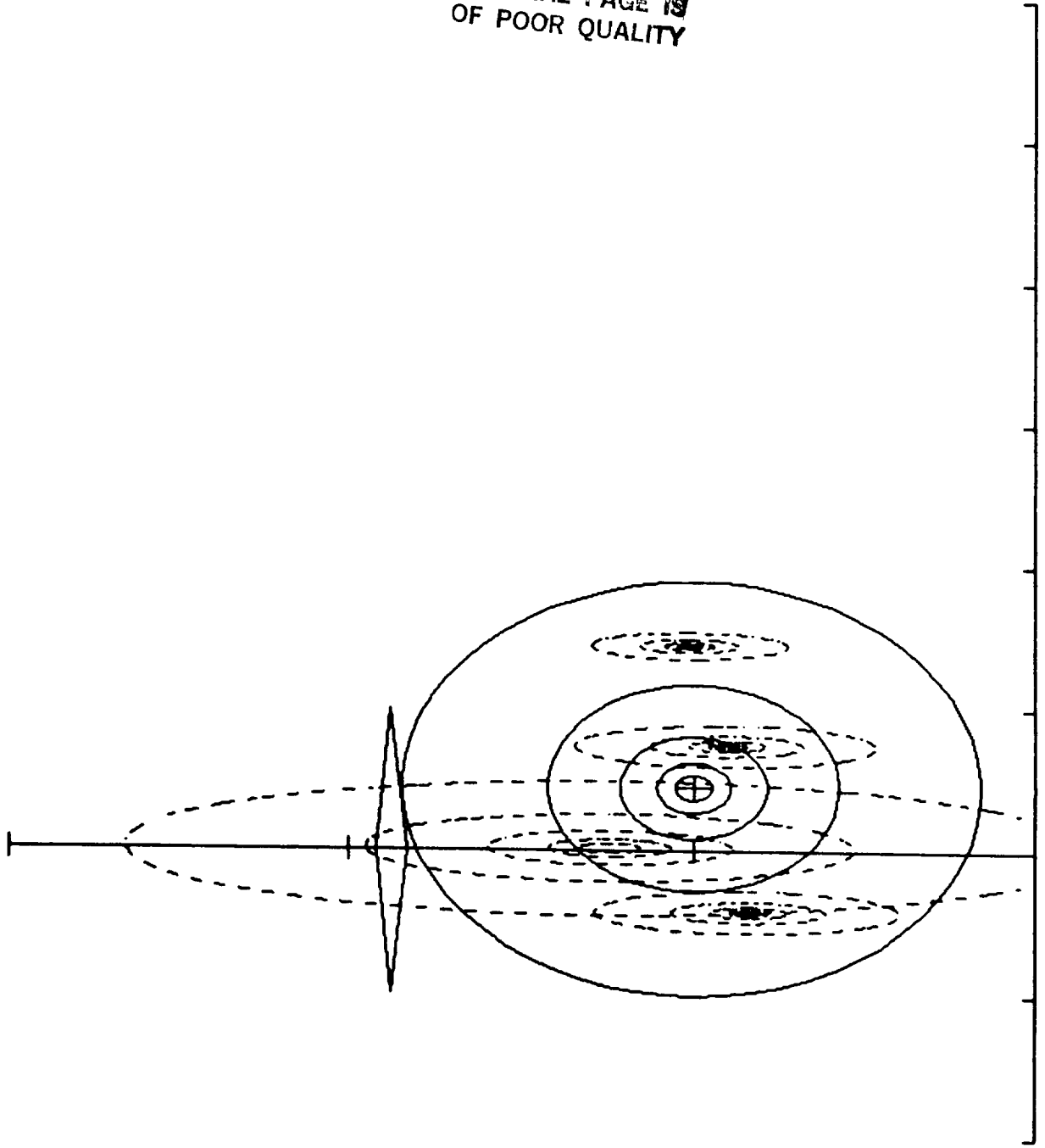


Figure 21. Equivalent Gaussian distribution for the example test case in Ref. 16

## 7. CONCLUSIONS AND RECOMMENDATIONS

A computer code AGDISP has been developed which has the potential to reliably and efficiently predict the deposition of agricultural material released from rotary and fixed wing aircraft. This code computes the ensemble averaged mean motion of the material and the dispersion about this mean motion resulting from turbulent fluid fluctuations. These fluctuations result from turbulence generated by the aircraft itself or present normally in the atmosphere. Initial validation of the AGDISP predictions against deposition data taken behind a fixed wing aircraft is promising. Additional studies should be undertaken to confirm adequacy of the flow field modeling, particularly the helicopter wake downwash model, to assure acceptable accuracy of deposition predictions behind these aircraft.

## 8. REFERENCES

1. Reed, W. H.: An Analytical Study of the Effect of Airplane Wake on the Lateral Dispersion of Aerial Sprays. NACA Rep. 1196, 1954.
2. Trayford, R. S.; and Welch, L. W.: Aerial Spraying: A Simulation of Factors Influencing the Distribution and Recovery of Liquid Droplets. J. Agric. Engng. Res., 22, 1977, pp. 183-196.
3. Ormsbee, A. I.; Bragg, M. B.; and Maughmer, M. D.: The Development of Methods for Predicting and Measuring Distribution Patterns of Aerial Sprays. NASA CR-165652, January 1981.
4. Loats Associates: Selection of Candidate Aerial Spray Drift Models. USDA APHIS Contract No. 53-3294-1-24, February 1982.
5. Wickens, R. H.: A Technique for Simulating the Motion and Ground Effect of Aircraft Wake Vortices - With Particular Reference to the Aerial Spraying of Pesticides. National Research Council of Canada LTR-LA-186, November 1975.
6. Wickens, R. H.: Calculations of Wake Vortex Trajectories for Low Flying Spray Aircraft. National Research Council of Canada LTR-LA-215, July 1977.
7. Bilanin, A. J.; Teske, M. E.; and Hirsh, J. E.: Neutral Atmospheric Effects on the Dissipation of Aircraft Vortex Wakes. AIAA J., 16, 1978, pp. 956-961.
8. Jordan, F. L., Jr.; McLemore, H. C.; and Bragg, M. B.: Status of Aerial Applications Research Facility and the Langley Full Scale Wind Tunnel. NASA TM-78760, August 1978.
9. Morris, D. J.: Analytical Prediction of Agricultural Aircraft Wakes. ASAE Paper No. 78-1506, December 1978.
10. Teske, M. E.: Vortex Interactions and Decay in Aircraft Wakes. II: The Vortex Wake Computer Program. User Manual. A.R.A.P. Report No. 271, March 1976.
11. Teske, M. E.: Vortex Interactions and Decay in Aircraft Wakes. III: The Vortex Wake Computer Program. Programmer Manual. A.R.A.P. Report No. 271, March 1976.
12. Langmuir, I.; and Blodgett, K. B.: A Mathematical Investigation of Water Droplet Trajectories. AAF TR No. 5418 (Contract No. W-33-038-ac-9151), Air Technical Service Command, Army Air Force, Feb. 19, 1946.
13. Von Karman, T. D.; and Howarth, L.: On the Statistical Theory of Isotropic Turbulence. Proc. Roy. Soc. (A), 1938, pp. 164.
14. Lewellen, W. S.; and Teske, M. E.: Second-Order Closure Modeling of Diffusion in the Atmospheric Boundary Layer. Boundary-Layer Meteorology, no. 10, 1976, pp. 60-90.

15. Dennison, R. S.; and Wedding, J. B.: Determination of Evaporation Rates of Pesticide Droplets. Aerosol Science Laboratory, Colorado State University, July 1982.
16. Teske, M. E.: Computer Program for Prediction of the Deposition of Material Released From Fixed and Rotary Wing Aircraft. NASA CR-3780, 1984.
17. Donaldson, C. duP.; and Bilanin, A. J.: Vortex Wakes of Conventional Aircraft. AGARD-AG-204, May 1975.
18. Betz, A.: Behavior of Vortex Systems. NACA TM 713, 1933.
19. Bilanin, A. J.; AND DONALDSON, C. duP.: Estimation of Velocities and Roll-Up in Aircraft Vortex Wakes. J. Aircraft, vol. 12, no. 7, July 1975, pp. 578-585.
20. Lewellen, W. S.; Teske, M. E.; and Donaldson, C. duP.: Application of Turbulence Model Equations to Axisymmetric Wakes. AIAA J., no. 12, 1974, pp. 620-625.
21. Wilson, N. R.; and Shaw, R. H.: A Higher Order Closure Model for Canopy Flow. J. Appl. Meteor., vol. 16, 1977, pp. 1197-1205.
22. Donaldson, C. duP.: Construction of a Dynamic Model of the Production of Atmospheric Turbulence and the Dispersal of Atmospheric Pollutants. Workshop on Micrometeorology, ed. by D. A. Haugen, American Meteorological Society, Boston, MA, 1973, pp. 313-390.
23. Morris, D. J.; Croom, C. C.; Holmes, B. J.; and van Dam, C. P.: NASA Aerial Applications Wake Interaction Research. Presented at the 1982 Joint Technical Session, Am. Soc. of Agric. Eng. and Nat. Agric. Avia. Assoc., 1982



1. Report No. NASA CR-3779		2. Government Accession No.		3. Recipient's Catalog No.	
4. Title and Subtitle NUMERICAL STUDIES OF THE DEPOSITION OF MATERIAL RELEASED FROM FIXED AND ROTARY WING AIRCRAFT				5. Report Date March 1984	
				6. Performing Organization Code	
7. Author(s)  Alan J. Bilanin and Milton E. Teske				8. Performing Organization Report No.	
				10. Work Unit No. 505-45-43-02	
9. Performing Organization Name and Address  Continuum Dynamics, Inc. P.O. Box 3073 Princeton, New Jersey 08540				11. Contract or Grant No. NAS1-16031	
				13. Type of Report and Period Covered Contractor Report	
12. Sponsoring Agency Name and Address  National Aeronautics and Space Administration Washington, DC 20546				14. Sponsoring Agency Code	
15. Supplementary Notes  Langley Technical Monitor: Dana J. Morris					
16. Abstract  The computer code "AGDISP" ( <u>A</u> gricultural <u>D</u> ISpersal) has been developed to predict the deposition of material released from fixed and rotary wing aircraft in a single-pass, computationally efficient manner. The formulation of the code is novel in that the mean particle trajectory and the variance about the mean resulting from turbulent fluid fluctuations are simultaneously predicted. The code presently includes the capability of assessing the influence of neutral atmospheric conditions, inviscid wake vortices, particle evaporation, plant canopy and terrain on the deposition pattern.  In this report, the equations governing the motion of aerielly released particles are developed, including a description of the evaporation model used. A series of case studies, using AGDISP, are included.					
17. Key Words (Suggested by Author(s)) Aerial Applications Particle Trajectory Wake Interactions Crop Dusting			18. Distribution Statement Unclassified - Unlimited  Subject Category - 02		
19. Security Classif. (of this report) Unclassified		20. Security Classif. (of this page) Unclassified		21. No. of Pages 60	22. Price A04